SAFEGUARD MONITORING OF DIRECT ELECTROLYTIC REDUCTION

by

Abraham L. Jurovitzki

A thesis submitted to the faculty of
The University of Utah
in partial fulfillment of the requirements for the degree of

Master of Science

Department of Metallurgical Engineering

The University of Utah

December 2015

The University of Utah Graduate School

STATEMENT OF THESIS APPROVAL

The thesis of **Abraham L. Jurovitzki**

has been approved by the following supervisory committee members:

Michael F. Simpson	, Chair	**4/29/2015** Date Approved
Michael L. Free	, Member	**4/29/2015** Date Approved
Sang Mun Jeong	, Member	**5/4/2015** Date Approved

and by **Manoranjan Misra** , Chair of

the Department of **Metallurgical Engineering**

and by David B. Kieda, Dean of The Graduate School.

ABSTRACT

Nuclear power is regaining global prominence as a sustainable energy source as the world faces the consequences of depending on limited fossil-based, CO_2 emitting fuels. A key component to achieving this sustainability is to implement a closed nuclear fuel cycle. Without achieving this goal, a relatively small fraction of the energy value in nuclear fuel is actually utilized. This involves recycling of spent nuclear fuel (SNF)—separating fissile actinides from waste products and using them to fabricate fresh fuel. Pyroprocessing is a viable option being developed for this purpose with a host of benefits compared to other recycling options, such as PUREX. Notably, pyroprocessing is ill-suited to separate pure plutonium from spent fuel and thus has nonproliferation benefits. Pyroprocessing involves high-temperature electrochemical and chemical processing of SNF in a molten salt electrolyte. During this batch process, several intermediate and final streams are produced that contain radioactive material. While pyroprocessing is ineffective at separating pure plutonium, there are various process misuse scenarios that could result in diversion of impure plutonium into one or more of these streams. This is a proliferation risk that should be addressed with innovative safeguards technology.

One approach to meeting this challenge is to develop real-time monitoring techniques that can be implemented in the hot cells and coupled with the various unit operations involved with pyroprocessing. Current state-of-the-art monitoring techniques

involve external chemical assaying, which requires sample removal from these unit operations. These methods do not meet the International Atomic Energy Agency's (IAEA) timeliness requirements.

In this work, a number of monitoring techniques were assessed for their viability as online monitoring tools. A hypothetical diversion scenario for the direct electrolytic reduction process was experimentally verified (using Nd_2O_3 as a surrogate for PuO_2). Electrochemical analysis was demonstrated to be effective at detecting even very dilute concentrations of actinides as evidence for a diversion attempt.

TABLE OF CONTENTS

ABSTRACT ……. iii

LIST OF FIGURES …… vii

LIST OF TABLES ……..... ix

ACKNOWLEDGMENTS …… x

Chapters

1 BACKGROUND ...…… 1

1.1 Introduction …….. 1
1.2 Hydrometallurgical Reprocessing …… 2
1.3 Pyroprocessing…….…….... 3
1.4 Motivation …… 8

2 PROLIFERATION RISKS AND POLICY …….. 11

2.1 Policy Background …… 11
2.2 Pyroprocessing Safeguards Techniques ……. 14
2.2.1 Neutron Assay ……. 14
2.2.2 Gamma Ray Spectroscopy …….. 16
2.2.3 X-ray Techniques ……..... 18
2.2.4 Calorimetry …… 19
2.2.5 Emission Spectroscopy ……... 19
2.2.6 Absorption Spectroscopy ……..... 20
2.2.7 Electrochemical Methods ……..... 21
2.2.8 Chemical Assay …….. 22
2.2.9 Techniques Summary …… 23
2.3 Diversion Scenarios ……... 24
2.3.1 Head-End Fuel Treatment ……... 24
2.3.2 Electrorefining ……..... 25
2.3.3 Cathode Processing ……. 25
2.3.4 Oxide Reduction …… 26
2.4 Conclusions ……..... 29

3 ABSORPTION SPECTROSCOPY LITERATURE REVIEW……. 30

4 MOLTEN SALT ELECTROCHEMISTRY ……. 37

4.1 Introduction …… 37
4.2 Electrochemistry Theory …… 38
4.3 Application of Molten Salt Electrochemistry to Actinide Measurement …... 41

5 EXPERIMENTAL METHODS …… 43

5.1 Methods …….. 43
5.2 Materials …… 43
5.2.1 Spectroscopy Salt Preparation …… 44
5.3 Equipment and Procedures …… 45
5.3.1 Glovebox ……. 45
5.3.2 Chlorination Procedure ……... 46
5.3.3 Pelletization Procedure ……... 48
5.3.4 UV-Vis Spectroscopy Equipment and Procedure ……... 50
5.3.5 Electrochemical Test Assembly and Procedure …….. 51
5.3.6 Differential Scanning Calorimetry Equipment and Procedure …... 53

6 RESULTS AND DISCUSSION ……... 55

6.1 Introduction ……..... 55
6.2 Electrochemistry …… 55
6.3 Thermal Analysis ……... 65
6.4 UV-Vis Spectroscopy …… 70

7 SUMMARY …….. 72

REFERENCES .....……... 77

LIST OF FIGURES

Figures

1.1 Equipment used at INL in the treatment of EBR-II spent nuclear fuel ……... 4

1.2 Schematic of direct electrolytic reduction (DER) process …….. 7

2.1 Potential diversion pathways for a pyroprocessing facility …… 24

2.2 Calculated free energy change for reaction of UO_2 with various chlorides to form UCl_3 ……...……..... 27

2.3 Calculated free energy change for reaction of U_3O_8 with various chlorides to form UCl_3 ……...……... 28

2.4 Calculated free energy change for reaction of PuO_2 with various chlorides to form $PuCl_3$ ……...……. 28

5.1 Argon atmosphere glovebox ……. 45

5.2 Schematic of $ZrCl_4$ addition to LiCl-SrCl2-CsCl via trapping method ……. 47

5.3 Schematic of two stages chlorination of UO_2 in LiCl-$SrCl_2$–CsCl-$ZrCl_{4-x}$ salt at 923 K ……... 48

5.4 Stainless steel cup and Zr foil after one hour of submersion in molten salt at 923 K … ……... 49

5.5 UO_2-Nd_2O_3 pellet after sintering ……... 50

5.6 Schematic of UV-Vis spectroscopy experimental setup …… 50

5.7 Kerr furnace operating within the glovebox …….. 51

5.8 Schematic of electrochemical experimental setup ……. 53

5.9 The DSC/TGA unit used for thermal analysis of salt samples …….. 54

6.1 Images of salt ingot following electrochemical experiments …… 56

6.2 Cyclic voltammogram of LiCl-1 wt% $SrCl_2$- 1wt.% CsCl at 923 K ……. 57

6.3 Cyclic voltammograms at various scan rates of LiCl-$SrCl_2$-CsCl-UCl_3 after one hour of chlorinating with $ZrCl_4$ and Zr at 923 K……... 58

6.4 Plot of peak current versus square root of scan rate of LiCl-$SrCl_2$-CsCl-UCl_3 salt after one hour of chlorinating at 923 K. ……... 59

6.5 Cyclic voltammograms at various scan rates of LiCl-$SrCl_2$-CsCl-UCl_3 after two hours of chlorinating with $ZrCl_4$ and Zr at 923 K. ……. 60

6.6 Plot of peak current versus square root of scan rate of LiCl-$SrCl_2$-CsCl-UCl_3 salt after two hours of chlorinating at 923 K …….. 61

6.7 Cyclic voltammograms at 200 mV/s scan rate of LiCl-$SrCl_2$-CsCl-UCl_3 after one hour and two hours of chlorinating with $ZrCl_4$ and Zr at 923 K …….. 62

6.8 Cyclic voltammograms at various scan rates of LiCl-$SrCl_2$-CsCl-UCl_3-$NdCl_3$ after one hour of chlorinating with $ZrCl_4$ and Zr at 923 K …….. 63

6.9 Plot of U(III) peak current versus square root of scan rate of LiCl-$SrCl_2$-CsCl-UCl_3-$NdCl_3$ salt after one hour of chlorinating at 923 K …….. 64

6.10 Plot of Nd(III) peak current versus square root of scan rate of LiCl-$SrCl_2$-CsCl-UCl3-NdCl3 salt after one hour of chlorinating at 923 K ……... 64

6.11 DSC result of as-received LiCl and dried LiC ……. 66

6.12 TGA data from as-received LiCl and dried LiCl. …… 67

6.13 DSC result of as-received LiCl, LiCl-1 wt% $SrCl_2$ – 1 wt% CsCl and LiCl-$SrCl_2$-CsCl-$ZrCl_4$ salts ……... 68

6.14 DSC results of LiCl-$SrCl_2$-CsCl and LiCl-$SrCl_2$-CsCl-$ZrCl_4$-UCl_3 salt after one hour and two hours of chlorination …….. 69

6.15 DSC results of LiCl-$SrCl_2$-CsCl, LiCl-$SrCl_2$-CsCl-$ZrCl_4$-UCl_3 salt after one hour of chlorination and LiCl-$SrCl_2$-CsCl-ZrCl4-UCl_3-$NdCl_3$ salt after one hour of chlorination ……... 69

LIST OF TABLES

Tables

2.1 Summary of measurement methods suitable for application to pyroprocessing safeguards …… ……... 15

3.1 Major absorption peaks of transition metal ions in various molten salts ……... 32

3.2 Major absorption peaks of rare earth ions in various molten salts …… 33

3.3 Major absorption peaks of actinide ions in various molten salts ……... 34

5.1 Heating scheme for drying LiCl salt in a muffle furnace in open atmosphere …….. 44

5.2 Electrodes using for cyclic voltammetry of molten LiCl salts …….. 52

6.1 Free energies of formation and standard reduction potentials for chloride salts present in this study.....……... 56

6.2 Comparison of ICP-AES analysis and Berzins-Delahay equation fitting results for LiCl-CsCl-$SrCl_2$-UCl_3 after one hour of chlorination, LiCl-CsCl-$SrCl_2$-UCl_3 after two hours of chlorination and LiCl-CsCl-$SrCl_2$-UCl_3-$NdCl_3$ after one hour of chlorination . 65

7.1 List of chlorinating agents considered for reaction with actinide oxides …….. 75

ACKNOWLEDGMENTS

A great deal of thanks and appreciation goes to the members of my thesis committee. I am grateful to Dr. Free for providing me with my first research experience by allowing me to work in his research group as an undergraduate. I am grateful to Dr. Jeong for his hands-on and theoretical help with various aspects of my molten salt electrochemical experiments. I am grateful to Dr. Simpson for taking me on his research group, patiently working with me on running experiments, and kindly refining many versions of this manuscript. I owe a great deal of thanks to many lab mates. To this work a number of students contributed: Devin Rapplye and Milan Stika helped with the electrochemical experiments and Lauryn Hansen ran samples for DSC/TGA and ICP-AES analysis. Most importantly, the biggest thanks goes to my parents and sister for supporting and encouraging me throughout the many years I attended the University of Utah.

CHAPTER 1

BACKGROUND

1.1 Introduction

Many countries are pursuing development of nuclear power as a major, sustainable source of energy. Currently, nuclear power represents approximately 14% of the electricity generation worldwide.[1] Light water reactors (LWR) account for almost 90% of the installed capacity, with pressurized water reactors (PWR) contributing 5% of installed capacity. The majority of these reactors operate on an unsustainable once-through fuel cycle. Once the fuel is burnt-up to the desired level, the fuel is disposed of.

A key technical issue facing nuclear power sustainability is management of spent nuclear fuel. Currently in the United States, spent fuel from nuclear power plants and most legacy research reactors is stored onsite. In the 1960s and 1970s, the U.S. built reprocessing facilities at West Valley (NY), Barnwell (SC), and Morris (IL) with an intention to recycle actinides from commercial spent nuclear fuel. However, in 1977, the U.S. changed its policy towards reprocessing, and these plants were all shut down.[2] Focus then shifted to direct disposal of spent fuel into a deep geological repository. Nuclear waste repository projects have run into public opposition, unfortunately. For instance, the Yucca Mountain project in Nevada came under a great deal of public scrutiny. According to Government

Accountability Office, the project was eventual canceled in April 2011 for "policy reason and not technical reasons.[3]" Other countries such as the United Kingdom, France, Germany, Japan, South Korea, India, and Russia have chosen to reprocess spent nuclear fuel (SNF). Since it contains a large portion of still usable fissile material, the SNF can be reused after reprocessing. For instance, assuming a 40 GWd/t burnup for LWR fuel, the SNF still contains 96% U and 1% transuranics (TRU).[4] Moreover, a typical nuclear reactor generates 20 metric tonnes of SNF per year. There is also the issue of controlling and burning up nuclear material such as Pu-239. Additionally, a typical LWR produces approximately 0.2 g of Pu-239 per MW (thermal)-day, thus a 3000 MW (thermal) LWR can produce over 0.5 kg of Pu per day. A fast breeder, heavy water, or fast breeder optimally reflected can produce up to a 1 g of Pu-239 per MW (thermal)-day.[5] This represents a large amount of Pu that needs to be reprocessed and subsequently consumed to prevent proliferation. Therefore, the reprocessing of spent fuel is necessary. Although reprocessing does not completely negate the need for waste storage, it does minimize the space requirements, proliferation concerns, and storage duration requirements.

1.2 Hydrometallurgical Reprocessing

Hydrometallurgical-based reprocessing is a mature technology. It is amenable to certain types of nuclear fuels that have been typically cooled 10 years prior to reprocessing.[6] All commercial reprocessing plants in the world employ variations of the Plutonium-Uranium Extraction (PUREX)-based solvent extraction method. In this method, cut up spent fuel is dissolved in nitric acid. This dissolution of the fuel serves as a material input accountancy. Pu and U are extracted from the acid solution by a tributyl phosphate

containing organic phase. In general, metals in the +4 and +6 oxidation state are extracted. Additionally, there are a number of variations to PUREX under development: TRUEX[6], UREX[7], DIAMEX[8], SANEX[9] and UNEX.[10]

Several disadvantages of hydrometallurgical reprocessing are as follows:

- Organic phase breaks down from high radiation fields
- High volumes of liquid waste are generated
- Criticality issues arise due to the presence of hydrogen and carbon

However, it is from a nuclear proliferation risk standpoint that the greatest problem associated with PUREX is exposed. The PUREX process was originally designed for purifying Pu. Thus, it can be misused to separate out a weapons grade Pu. A promising alternative to hydrometallurgical reprocessing is pyroprocessing, which is not suitable for extracting pure plutonium from spent nuclear fuel.

1.3 Pyroprocessing

Pyroprocessing is a reprocessing technology that is drawing a great deal of interest internationally and currently being actively evaluated by the United States, Japan, South Korea, India, and Russia. Pyroprocessing involves high-temperature electrochemical and chemical processing of used nuclear fuel in a molten salt electrolyte.[11] Figure 1.1 depicts the flowsheet and reagents used at Idaho National Laboratory for their application of pyroprocessing to treat spent fuel from Experimental Breeder Reactor-II.

Reprocessing starts with incoming fuel being declad and chopped into manageable segments. The major separation unit operation occurs in an electrorefiner where declad SNF is submerged within an anode basket into molten eutectic lithium chloride-potassium

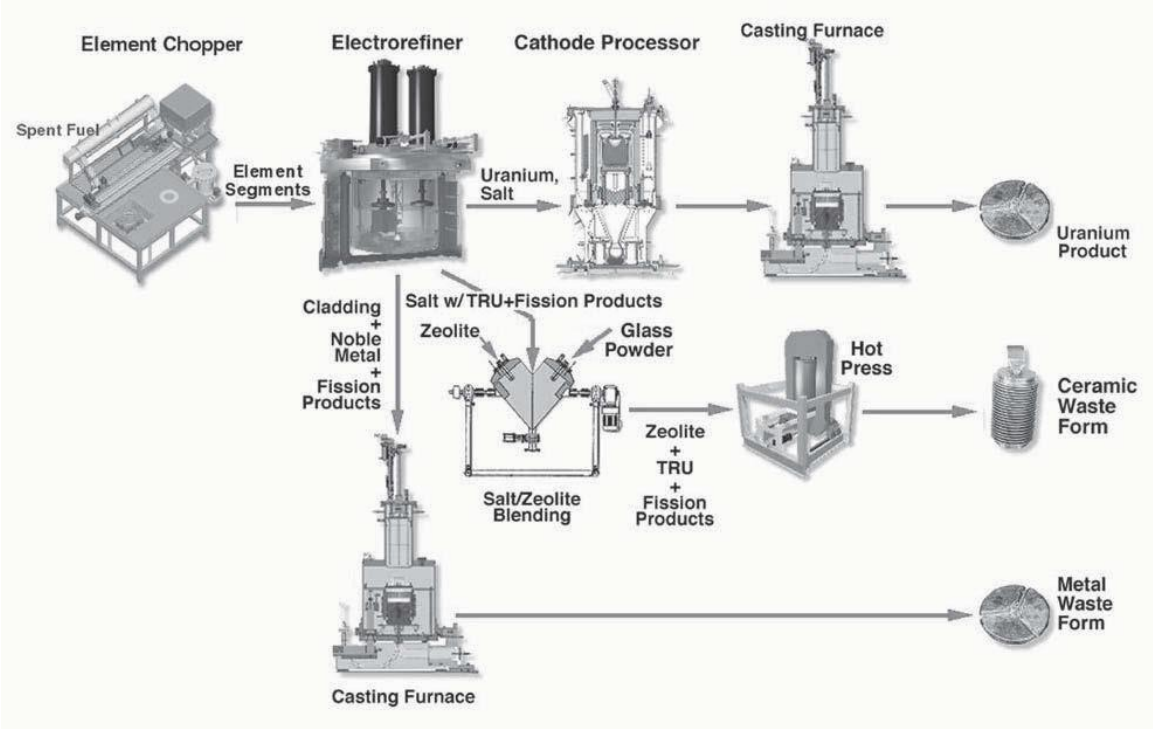

Figure 1.1: Equipment used at INL in the treatment of EBR-II spent nuclear fuel.[12]

chloride (LiCl-KCl) chloride salt. The uranium within the anode basket is driven electrochemically to a solid cathode.

More specifically, U metal is electrochemically oxidized to U^{3+} and simultaneously reduced to U on the cathode:

$$U^{3+}{}_{(LiCl\text{-}KCl)} + 3e^- \rightarrow U_{(s)} \qquad (1.1)$$

Pu and other active metals are spontaneously oxidized. For instance, the oxidation of Pu is thermodynamically spontaneous:

$$Pu + UCl_{3\,(s)} \rightarrow PuCl_{3\,(s)} + U \qquad \Delta G^\circ = -93 \text{ kJ/mole} \qquad (1.2)$$

When it is necessary to extract Pu and other minor actinides from the salt, a liquid cadmium cathode can be inserted into the salt and used to promote co-deposition of U/TRU. The cadmium serves to thermodynamically stabilize Pu and other TRUs, preventing the oxidation reaction listed above. The cathode products are further purified by salt distillation and thermal consolidation. Salt must be distilled off both cathode products. Additionally, cadmium is distilled off the TRU cathode. The resulting purified metal streams can be refabricated into nuclear fuel by injection molding. Accompanying the main processes are several waste treatment steps. For example, the salt can be treated via drawdown to remove actinide chlorides. Fission products such as rare earth, alkaline, and alkaline earth metals can be then selectively separated via a variety of processes such as zeolite ion exchange, oxygen sparging, zone freezing, and phosphate precipitation. These processes allow the LiCl-KCl eutectic salt to be recycled back into the electrorefiner, while waste forms containing concentrated fission products are sent out for permanent disposal.[13]

Pyroprocessing has several important benefits over hydrometallurgical processing:

- No radioactive liquid waste is generated.
- All radioactive wastes streams are solid at ambient temperatures and readily convertible into stable waste forms.
- Short-cooled nuclear waste can be processed because of the radiation-resistance of the process chemicals used.
- The facility is inherently compact and can readily be co-located with a nuclear power plant.

Proliferation resistance wise, the inability to generate weapons grade Pu is extremely important. Any Pu stream from pyroprocessing would require additional refining via PUREX. Also, pyroprocessing is quite versatile as far as the types of fuel it can reprocess. This includes both oxide light water reactor (LWR) fuel[14] and metallic breeder reactor fuel.[13]

The actual electrorefining operation requires that the fuel feed be in the metallic state. Thus, head-end processing is necessary to reduce spent oxide fuels to metals prior to electrorefining.[14,15] Oxide fuel is first declad, which can be accomplished either via simple chopping and mechanical crushing of the fuel or via a high temperature oxidation process known as voloxidation.[16] Voloxidation reacts air or O_2 with segmented pieces of spent fuel at high temperatures. UO_2, the main constituent of the fuel, is oxidized to U_3O_8. The primary reaction is as follows:

$$3UO_2 + O_{2(g)} = U_3O_8 \qquad (1.3)$$

This oxidation process causes the spent fuel to expand and pulverize. Volatile fission products such as tritium, krypton, and iodine are also released and can be captured via off-gas treatment systems.

Subsequently, a direct electrolytic reduction (DER) process introduced at Argonne National Lab is utilized to reduce the fuel.[17] This DER process is depicted in Figure 1.2. In this process, the declad oxide fuel is loaded into a cathode basket lined with porous metal and immersed into a molten salt electrolyte consisting of LiCl-1% wt. Li_2O electrolyte at 923 K. The oxide fuel, contained within a cathode basket, is electrolytically reduced. Rare

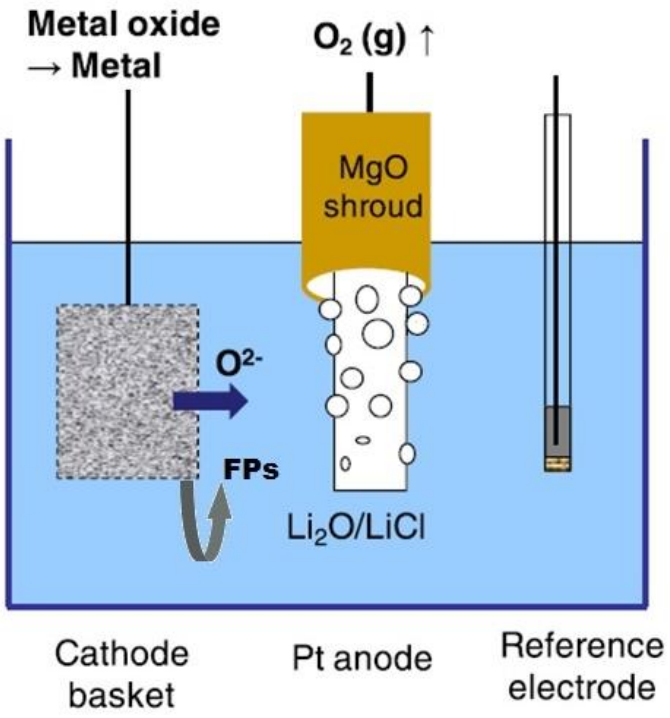

Figure 1.2: Schematic of direct electrolytic reduction (DER) process.

earths, transuranics, and uranium are reduced to metal. Reduction occurs indirectly where lithium forms followed by chemical reduction occur via the following reactions:

$$\text{Cathode: } 4Li^{+}_{(LiCl)} + 4e^{-} \rightarrow 4Li_{(\ell)} \quad (1.4)$$

$$\text{Anode: } 2O^{2-}_{(LiCl)} \rightarrow O_2\,(g) + 4e^{-} \quad (1.5)$$

$$\text{Net cell reaction: } 2Li_2O_{(LiCl)} \rightarrow 4Li_{(\ell)} + O_2\,(g) \quad (1.6)$$

$$\text{Chemical reaction: } 4Li_{(\ell)} + MO_{(s)} \rightarrow M_{(s)} + Li_2O_{(LiCl)} \quad (1.7)$$

Or directly by electrolytic reduction via the following reactions:

Cathode: $MO_{2\,(s)} + 4e^- \rightarrow U_{(s)} + 2O^{2-}$ (1.8)

Anode: $2O^{2-} \rightarrow O_2\,(g) + 4e^-$ (1.9)

Net cell reaction: $MO_{2\,(s)} \rightarrow M_{(s)} + O_2\,(g)$ (1.10)

Afterwards, this reduced fuel can be sent to an electrorefiner for electrochemical purification of the uranium or extraction of a U/TRU actinide product. Researchers at Idaho National Laboratory have demonstrated 99.7% conversion of UO_2 to U metal and comparable values for Pu and Np in lab-scale DER tests.[11]

The fuel also contains a number of fission products that are chemically active in the LiCl-Li_2O salt such as cesium, barium, strontium, rubidium, tellurium, and iodine. These fission products react to form salts (chlorides in the case of Cs, Ba, Sr, and Rb), which then diffuse from the fuel and accumulate in the electrolyte during electrolytic reduction. The concentration levels of these highly radioactive soluble species must be maintained below a threshold to ensure optimal operation of the DER process.

1.4 Motivation

While normal oxide reduction operations have long been considered to be a low proliferation threat due to the immobility of actinides—they remain in the cathode basket as they are converted from oxides to metals. However, all potential abnormal conditions much be considered when assessing the threat of the process being used to divert fissile material. It has been hypothesized that conversion of the actinides from oxides to chlorides is chemically feasible and might be made to occur in the DER process under abnormal conditions. This would make it possible for fissile actinides to be diverted via the DER

salt disposal path. The introduction of a chemically reactive chloride such as $ZrCl_4$ could cause U and Pu to diffuse into the LiCl electrolyte. From a material control and accountability perspective, there needs to be adequate assurance that no actinides were partitioned into the electrolyte. While such partitioning would be outside the realm of normal operations, it can be viewed as a threat since the electrolyte is disposed as waste when the fission product concentrations reach a maximum allowable level. On the off-chance that the operator finds a way to chemically partition the actinides from the cathode basket into the salt, a process monitoring method is needed to safeguard against such a diversion scenario.

Thus, oxide reduction operations require some type of process monitoring to ensure that the diversion has not taken place. Salt sampling and destructive analysis (DA) via external ICP-MS and ICP-OES can be effective for this purpose.[9,11] This requires radioactive salt samples be removed from hot cells and be sent to an analytical lab. This postprocess analysis does not meet timeliness standards of the IAEA.[12] Moreover, a discrepancy in material balance of actinides (nuclear material accountancy) could potentially be a false alarm and unnecessarily cause a commercial operation to be shut down for IAEA inspection. Real-time or near-real-time monitoring techniques are, thus, needed to prevent diversion of fissile actinides from the DER process. It is hypothesized that chemical oxidation of uranium and transuranics into the electrolytic salt needs to be detected and thus to be deterred. Such real-time process monitoring data could be used in an integrated approach called Signature Based Safeguards (SBS) to maximize the probability of detection of a diversion occurrence.[18] SBS would integrate several different online monitoring signals in an algorithm that would determine if there is enough indication

for inspectors to be alerted. This objective of this thesis is to assess the feasibility of a number of process monitoring methods for oxide reduction that could be used by an SBS system. Specifically, UV-Vis spectroscopy, thermal analysis, and voltammetry have been studied with the results presented in this thesis.

CHAPTER 2

PROLIFERATION RISKS AND POLICY

2.1 Policy Background

A major hurdle in the US and internationally to acceptance of pyroprocessing is the undeveloped nature of the safeguards approach that would be utilized. The IAEA literally does not know how they would inspect and analyze a pyroprocessing plant to detect diversion of nuclear material. There is a multitude of final and intermediate pyroprocessing process streams that hypothetically present a proliferation risk. Overall, safeguards must be in place to insure all U/TRU is accounted for after the batch-wise pyroprocessing operation is completed. More specifically, the International Atomic Energy Agency (IAEA) has a timeliness detection goal to detect the diversion of 8 kg of Pu in one month.[19] However, IAEA currently has no specific safeguard protocols or methodology in place for pyroprocessing. Their objective would be to implement nuclear material accountancy (NMA) and use a sequence of sampling and destructive analysis to determine the amount of material unaccounted for (MUF) and determine if and when the MUF exceeds the 8 kg significant quantity (SQ). However, there is substantial hold-up of Pu and other actinides in vessels containing molten salt. Furthermore, there is no direct experimental method to determine the amount of Pu and other fissile material entering the process. Spent Fuel

composition is variable based on initial composition, burnup, decay, and spatial position. Alternatives to NMA have been explored by a number of researchers that would include (1) determining possible proliferation pathways, (2) identifying the most vulnerable process step(s), (3) determining indications of possible material diversions, and (4) and determining indications of misuse of the facility for purposes other than declared.[19]

Since pyroprocessing of SNF is not yet commercialized, there is currently a window of opportunity to develop safeguards methods that can be practically and reliably utilized in future reprocessing complexes. The insight learned from safeguarding PUREX (aqueous)-based facilities may be applicable. However, there are some stark differences and challenges associated with safeguarding pyroprocessing operations.

A Sandia National Laboratory study pointed out the following four material accountancy challenges introduced by pyroprocessing:[20]

1. Lack of Accountability Tank: Due to the nature of pyroprocessing, there is no accountability tank at the front end of operation. The dissolution of SNF is coupled with cathode extraction. Thus, an initial actinide content measurement is not possible.
2. Inability to Flush Out the Plant: To extract the U/TRU product, TRU content must be built up to a certain level. Thus, a flush out of an electrorefining unit is not possible.
3. Electrorefiner Inventory: Actinide inventory is largest within the electrorefiner, a low uncertainty analytical technique is needed to measure the content. A well-mixed representative sample of the salt must be assayed.

4. Product Measurements: Unlike aqueous plants that have output accountability tanks with the final liquid product, pyroprocessing plants output solid streams. Compositional analytical techniques with high certainty (99%) are need.

The Global Nuclear Energy Partnership Technology Development Plan pointed out a few technical gaps that need to be filled to reduce the proliferation risk of pyroprocessing.[21] The U, Pu, and MA (minor actinide) content of the feed material needs to be determined by non-destructive assay (NDA). Also, techniques for (NDA or DA) high precision assay of final product ingots need to be developed. Finally, improved NDA techniques need to be developed for assaying salt and other actinide contaminated waste.

In contrast to NMA, a different method to mitigate proliferation of nuclear material is processing monitoring. Process monitoring entails analysis of real-time signals from various reprocessing unit operations. Process control measurements such as flowrates, density measurements, and concentrations would be monitored. Once a data set with normal activity signals is established, a comparison can be made to real-time signals. Analyzing the output measurements of multiple sensors through a statistical algorithm would detect abnormal operations. Abnormal activity signals would trigger a complimentary inspection. However, for international inspectors to accept these signals, separate, tamper-proof instruments are needed to measure and process the various signals.

One specific safeguards approach based on process monitoring is called Signature Based Safeguards (SBS).[18] SBS aims to incorporate potential diversion scenarios into physics-based models rather than using statistical inferences. By using physics-based models, there is the potential to minimize false alarms and to more accurately pinpoint anomalous activity. One example of how SBS could be implemented was recently

demonstrated when various electrorefining conditions were simulated followed by modeling of the neutron emission from the cathode products.[22] A combination of electrochemical monitoring and neutron counting appears to be promising for detection of abnormal ER runs that could be used to divert plutonium from the process.

2.2 Pyroprocessing Safeguards Techniques

There are number of significant safeguards-significant measurements that are implemented or can be implemented in the nuclear reprocessing industry. The monitoring of solid and room temperature liquid streams is well-developed while the monitor of high temperature streams is undeveloped. The safeguard techniques that are well-developed are well-suited for NMA which as mentioned before ideal for monitoring pyroprocessing. Table 2.1 summarizes the significant safeguards techniques and their usefulness for pyroprocessing safeguards. A more detailed description of these techniques is given in the sections that follow.

2.2.1 Neutron Assay

Neutrons are electrically negative particles with a mass identical to protons. Since neutrons have a mass, they can penetrate high-density material stored in large containers. Neutron emission, both from spontaneous and induced fission, is useful signal for assay of nuclear material.

Passive neutron counting involves quantifying the total neutron emission rate of an item or sample without inclusion of a neutron source. It represents spontaneous neutron emission either from decay or fission. A detector within a shielded well can count neutron

Table 2.1: Summary of measurement methods suitable for application to pyroprocessing safeguards

Technique	**Material Type**	**Pyroprocessing Online Monitoring**
Neutron Assay	Solids	No
Solid State Gamma Ray Spectroscopy	Solids	No
Digital Cloud Chamber	Solids, liquids and molten salts	Yes
XRF/KED	Liquids	No
Calorimetry	Solids	No
Emission Spectroscopy	Liquids and molten salts	Yes
Absorption Spectroscopy	Liquids and molten salts	Yes
Electrochemical Methods	Liquids and molten salts	Yes
Chemical	Liquids	No

coincidences from a sample. In the SNF, curium (Cm) isotopes are the major emitters of neutrons from spontaneous fission. Thus, a gross neutron count is measuring mostly Cm.[23] It has been proposed that the Cm/Pu ratio should remain constant throughout the process and can be determined via select sampling and destructive analysis (DA). If this were the case, then counting of neutrons from Cm could be used to also infer Pu mass in any given sample. However, there is substantial doubt that the Pu/Cm ratio remains the same based on differences in electrochemical properties. Also, this neutron balance technique is only accurate if the chopped SNF is homogenized prior to the NDA measurement. Since axial fuel rod burnup varies, incorporating a homogenizing step is critical for an accurate analysis. This additional step adds complexity and may cause delay for reprocessing operations.

Active neutron assay techniques induce fission using a neutron source and are used to assay for ^{235}U. Usually a similar setup as with passive neutron counting is utilized. However, special hardware and software is used to discern the neutrons from the specimen and the source. AmLi is a commonly used neutron source which can induce fission in ^{235}U.

AmLi has a mean neutron energy of 0.5 MeV, which is below fission threshold of 1 MeV for ^{238}U. Thus, an active well coincidence counter can assay kg quantities highly enriched U (HEU) to 1-5% and lightly enriched U (LEU) oxides or pellets to 5-10% in 1000 s.

When a nucleus fissions, there is a small percentage of neutron emissions that is delayed by a few seconds to a minute. Using a neutron source to irradiate a sample for 1-10 s, a delay neutron count can be conducted. Units using this active-decay technique can assay 200-L waste salt drums with 5-50% accuracy and product or scraps can to 1-2% accuracy.

Several systems that incorporate active, active-decay, and passive have been shown to be effective for assay waste drums. Differential die-away technique (DDT), which is used by U.S. and European waste generator sites, detects limits as low as a few 10s of mg of ^{235} U and ^{239} Pu in 208-L drums. DDT and the more advanced combined thermal-epithermal neutron (CTEN) technologies have the capability of detecting hidden SNM in waste even if it is shielded.

2.2.2 Gamma Ray Spectroscopy

The decay of nuclear material nuclides usually involves emission of alpha or beta particles and high energy photons. Gamma rays, with energies of tens to thousands of keV, are emitted when a nucleus changes energy states. Moreover, gamma rays have a discrete energies and intensities for each nuclide. Plutonium-239 emits gamma rays with characteristic energies at 414 keV. These energy signatures, with proper interpretation, provide relative isotopic composition and mass measurement. Gamma ray spectroscopy is a technique used to capture and analysis these high-energy photons.

Resolution of gamma ray spectra is highly dependent on detector type and configuration. For instance, germanium (HPGe) detectors offer great resolution but must be cooled to 77K. Similarly, CdTe detectors also require cooling albeit not as low, only to ambient temperature. This cooling requirement negates solid-state gamma spectroscopy's practically for online monitoring of molten salt pools. This relegates solid-state gamma ray spectroscopy techniques for precise analysis to solid streams such as homogenous SNF samples and cooled DER and ER salts.

An interesting alternative to solid-state gamma ray detector is a detector based on a Wilson cloud chamber, a digital cloud chamber, being researched at INL.[24] The cloud chamber is a sealed container filled with a supersaturated liquid or gas. When a radiation particle enters the chamber, it ionizes the surrounding atoms. Condensation occurs around these ions, thus streaks are formed. The type and energy of radiation particle can be identified based on the size, width, and length of these streaks. Several high-resolution cameras capture these streaks and convey this information to an inverse spectroscopy algorithm. With sufficient counts, a calculated location and quantity of plutonium in SNF is theoretically determinable. Since cameras can be channeled through fiber optics, a digital cloud chamber is essentially a mechanical device with no electronic components that can be harmed by radiation.

Nuclear materials attenuate (absorb and scatter) their own gamma rays due to their high density. In far-field assay, a gamma ray source is used to correct for this attenuation. By directing a known gamma ray source, an attenuation correction factor is quantified for a given sample. By integrating this technique with the principles of tomography, tomographic gamma-ray scanner (TGS) was developed to scan Pu-or U-bearing samples

up to 208L. TGS produces numerous volume elements scans by rotating and vertically and horizontal translating a sample. These volume elements are compiled into a 3D model. TGS has demonstrated to assay Pu to ± 2.6% in ER salt.[25]

2.2.3 X-Ray Techniques

K-Edge densitometry (KED) is based on passing a highly collimated x-ray through a sample and observing the characteristic absorption. An X-ray with enough energy will liberate one of the K-shell electrons, which will result in a sharp increase in the rate of x-ray absorption in the sample material and an x-ray intensity drop (K-edge drop) at the x-ray detector. This technique requires a sample be dissolved in an aqueous matrix. A 10 % uncertainty in total Pu content is associated with this measuring technique.[26]

X-Ray fluorescence (XRF) stimulates a characteristic K x-ray to be emitted from a sample after bombarding a sample with an x-ray or γ-ray beams. This can yield a Pu/U ratio or after calibration a quantitative result. Thus, solutions of dissolved MOX can be assayed.

A hybrid system combining KED and XRF, Hybrid K-Edge (HKED), shows better accuracy than individual systems. A single x-ray source is used for both the K-edge absorption and the fluorescence excitation analysis. Dissolved MOX solutions have been assayed to precision of 0.2% to 1% for samples containing as little as 2 g/L. Again, this combined technique requires a sample be taken out of a hot cell and dissolved in an aqueous matrix. This is problematic for a pyroprocessing safeguards due to timeliness requirement and the desire for online monitoring.

2.2.4 Calorimetry

Spent fuel contents a number of radioactive elements that emit electromagnetic particles. Alpha emission is absorb and stopped surround matrix. For example, a 5-MeV α particle in solid matrix can travel less than 10 μm, thus the energy that is dissipated as heat.[5] Varying isotopes of plutonium produce 2-12 W/kg of heat. Radiometric calorimetry is a technique that measure such heat output of nuclear material. Plutonium as well as more recently kilograms of uranium and neptunium are measureable. Since the matrix of the material does not interfere with measurements, calorimetry is the most accurate and precise nondestructive plutonium measurement technique. A solid-state calorimeter system has relative standard deviation of six measurements of 0.11%. However, calorimetry requires thermal equilibrium to be reach in a sample for measurement to be taken. The equilibration is time-consuming, taking up to eight hours or longer. Furthermore, calorimetry units are bulk units thus not readily applicable to international safeguard inspection work.

2.2.5 Emission Spectrophotometry

Emission spectroscopy is based on stimulating a characteristic photon emission by using a light source. Time-Resolved Laser Fluorescence Spectroscopy (TRFS) excites ions with a laser and measures the fluorescence as a function of time. Lanthanides and actinides in LiCl-KCl have been tested with TFRS at low level (< 0.5 wt%) with a 5% uncertainty.[27] Additionally, TRLFS proves information about the oxidations state of these ions. For safeguards application, salt samples must be extracted and transferred to a windowed furnace within a hot cell. To the spectrometry furnace, a laser light and resulting fluorescence signal need to be channeled in and out of the hot cell via fiber optics.

Laser-induced breakdown spectroscopy (LIBS), an atomic emission spectroscopy method, uses a highly energetic laser pulse as an excitation source. The laser forms a plasma which atomizes and excites samples. A high-resolution spectrometer can resolve thousands of peaks that can be associated with specific elements in the sample and used to quantify their concentrations.[28] LIBS has the potential to monitor molten salt pools in a hot environment by channeling laser light in and resulting light emission out via fiber optics.

2.2.6 Absorption Spectrophotometry

Absorption spectroscopy can employ individually or combinations of infrared, visible, and ultraviolet light absorbance for samples subject to light transmission. In theory, this can be applied to molten salt samples such as those found in oxide reduction and electrorefiner systems. Salt samples must be extracted and transferred to a windowed furnace within a hot cell and a dedicated light source and spectrometer that are channeled through fiber optics into the hot cell. The concentration of an ionic species can be established by using a calibration curve based on the Beer-Lambert law. The Beer-Lambert Law can be expressed as follows:

$$A = -\log (I/I_0) \tag{2.1}$$

where A, absorbance, is measured in terms of I_0 and I are intensities of incident light and transmitted light.

Numerous chloride solvent and solute combinations have been tested.[29,30] Notably, the U and RE content of a simulated spent LWR fuel dissolved in eutectic LiCl-KCl were found with 1% and 5% uncertainty, respectively.[30]

Raman spectroscopy operates by having a given substance shift a transmitting laser's energy. This shift allows for the observation of vibrational, rotational, and other low-frequency modes. These modes convey structure information about the sample and have been demonstrated on molten salts.[31] Raman spectroscopy potential could yield information that is complementary to UV-Vis-IR spectroscopy by giving additional information on certain species that cannot be resolved by absorption spectroscopy.

2.2.7 Electrochemical Methods

There are different electrochemical methods suited for various DER and ER constituents. Generally, these methods are online monitoring techniques and can provide live data to the IAEA if the signal can be authenticated. A common electrochemical method to employ is cyclic voltammetry (CV) which can measure concentration of various ionic species in ER and DER salt. Potential is ramped repeatedly between to vertex potentials at a constant scan rate. This potential change allows for the measure of both reduction and oxidation. Based on half-cell potentials and reduction-oxidation chemistry, relative concentrations of ionic species are indicated by resulting current peak height.

There are several other electrochemical methods being research. Square wave voltammetry (SWV) is being research as another method to measure actinide concentration in a melt.[20,32] SWV used waveforms that consist of staircase scan.[33] Current is sampled during the end of the pulses and the end of staircase steps. SWV is more sensitive to faradic

current, thus low concentration levels are detectable. Anodic stripping voltammetry (ASV) is also being developed as a technique to measure actinide levels on electrorefining cathodes.[34] ASV utilizes a bulk electrolysis step to preconcentrate metal ions on an electrode and subsequently strips them off.[33] This technique has been shown to analysis aqueous solution down to 10^{-10} to 10^{-11} M. A potentiometric sensor technology that uses a reference electrode with a fixed actinide concentration is being researched at INL for determining Pu^{3+} ion concentration in salt.[20] This technology's measurement uncertainty is currently unknown, as it has yet to be fully developed for actinide measurements. To date, it has largely been tested using gadolinium as a surrogate for plutonium.

Electrorefiner operating parameters can also be used as indicators of process misuse. If dual-use sensors for both process control and safeguards are not acceptable in terms of safeguards requirements, separate sensors can be installed.[32] For example, cell potential and cell current sensors could be independently installed by inspectors. The cell potential can be measured by connecting probes to the anode and cathode electrodes. Cell potential can be used to determine what ionic species the electrorefiner operator is electrorefining from the anode basket. Cell current measurement can provide insight into the rate of material being electro-transported to the cathode. The integral of current over a time range should be proportional to the amount of material depositing on the cathode. A low value for the integrated current for a given electrorefiner may indicate incomplete processing followed by subsequent material diversion.

2.2.8 Chemical Assay

There are several chemical assay techniques that are very accurate (1-5% uncertainty) but require samples be tested outside the reprocessing hot cell. These

techniques still have merit and a role in verifying processing stream compositions. For chemical assays to be accurate, homogenization of the stream must be performed. For instance, ingot sample assaying is a viable option with low uncertainty for verifying TRU/U and U ingot composition.[20] Mass spectrometry (MS) is an analytical technique that produces spectra of the masses of the atoms that comprising a sample. These spectra can show elemental or isotopic composition of a sample. An MS technique often used for SNF analysis is inductively coupled plasma mass spectrometry (ICP-MS).[35] ICP-MS ionizes a sample producing mass spectra. The technique is very accurate (1-5% uncertainty) and sensitive; however, its major drawback is that it is very difficult to be applied to on-line or in-situ measurement of process material.[29] Salt samples need to be removed from a hot cell, completely dissolved in an aqueous matrix, and diluted for ICP-MS analysis.

2.2.9 Techniques Summary

Overall, there is a wide variety of technology to safeguard future pyroprocessing facilities. Neutron, gamma, x-ray, and calorimetry techniques are well-developed technologies for analysis of bulk solid streams such as chopped SNF, metal waste forms, cathode product, and final U/TRU ingots. Chemical, electrochemical, and spectroscopic techniques are geared toward analysis of small sample size and can detect minute quantities of chemical species present. Moreover, techniques adaptable for near real time accountancy are electrochemical techniques, LIBS, emission spectroscopy, and absorption spectroscopy. SBS adaptable techniques have mostly been demonstrated on the lab scale. Further development is needed to mature the technology sufficiently to meet the stringent accuracy and speed that is required by the IAEA.

2.3 Diversion Scenarios

To develop the appropriate safeguards technology, each step in the pyroprocessing flowsheet must be analyzed for vulnerabilities and hypothetical diversion scenarios. There are a number of hypothetical scenarios for misuse and diversion of nuclear material during pyroprocessing. Some examples of hypothetical diversion scenarios are listed below and graphically represented in Figure 2.1. Note that there have been no published accounts of verified diversion scenarios—not surprising, since such information would certainly be tightly controlled.

2.3.1 Head-End Fuel Treatment

Spent fuel assembles must be declad and chopped into pieces suitable for rapid dissolution via electrochemical oxidation. During this mechanical process, an operator could remove portions of SNF and add depleted uranium oxide to mask its removal.

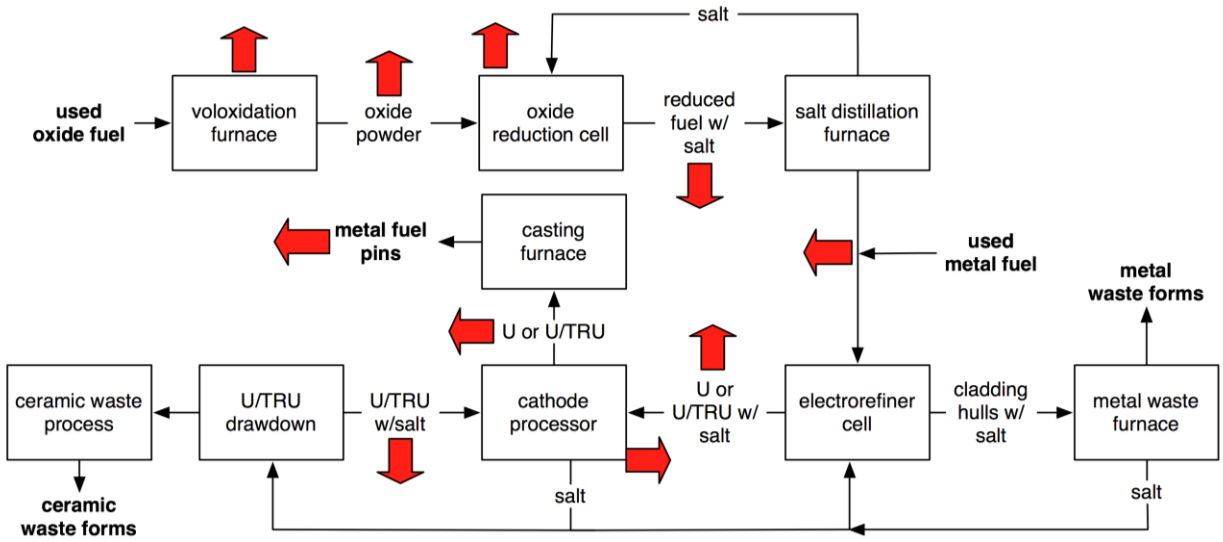

Figure 2.1: Potential diversion pathways for a pyroprocessing facility. Red arrows indicate diversion pathways.

Afterwards, in theory, the removed SNF could be sent to a clandestine facility for extracting weapons usable material.

Another possible diversion scenario would be the partial fluorination of UO_2 and other actinides to volatile flurides such as UF_6. During the voloxidation process a flurorinating agent such as gaseous bromine pentafluoride or solid ammonium bifluoride could be introduced. The actinide gases could be subsequently be collected.

2.3.2 Electrorefining

Molten salt pools present a high risk for misuse and diversion of nuclear material. In the ER process, if the Pu/U ratio in the salt is sufficiently high, the operator can codeposit metallic U and Pu at the cathode. Salt samples from the process can be taken by IAEA inspector and analyzed via a number of methods, which should serve of an indicator of such a diversion scenario. However, it would be easy for the operator to quickly replenish the UCl_3 inventory in the salt to cover up the diversion scenario before an inspector could have a sample taken.

2.3.3 Cathode Processing

During thermal consolidation and distillation of the cathode product, a chloride compound could be added to form chlorinate actinides which would then partition into the salt phase that separated from the metal via vacuum distillation. The distilled salt could be subsequently stripped of its actinide content via a reduction reaction.

2.3.4 Oxide Reduction

In the direct electrolytic reduction (DER) process—also known as *oxide reduction*, a credible diversion scenario is the chlorination of uranium and plutonium oxides. An operator could add a reactive chloride species to the OR melt which could hypothetically cause actinide oxides to chlorinate. This scenario was corroborated by both a paper by Sakamura[36] and HSC Chemistry 7.1 reaction equilibria calculations (see below). Once chlorinated, these actinides would dissolve into the LiCl salt. It was assumed that enough of the respective chloride would need to be added to first react with the 1% Li_2O present in the LiCl salt. A single chloride could be used to reduce lithium oxide and actinides or combination to better mask the byproduct metal oxide formation.

Equations 2.2-2.19 were input into HSC Chemistry 7.1 and all show favorability towards the forward reaction between 773 K (500°C) and 1073 K (800°C). Results are reasonable approximations, since the reaction would take place in a molten LiCl medium. Figures 2.2 - 2.4 show the calculated Gibbs free energy for a number of chlorination reactions (Equations 2.2-2.19) with UO_2, U_3O_8, and PuO_2.

$$4UO_2 + 3ZrCl_4 + Zr = 4UCl_3 + 4ZrO_2 \quad (2.2)$$

$$4UO_2 + 3TiCl_4 + 5Ti = 4UCl_3 + 8TiO \quad (2.3)$$

$$3UO_2 + 3AlCl_3 + Al = 3UCl_3 + 2Al_2O_3 \quad (2.4)$$

$$2UO_2 + WCl_6 + W = 2UCl_3 + 2WO_2 \quad (2.5)$$

$$3UO_2 + 3VCl_3 + V = 3UCl_3 + 2V_2O_3 \quad (2.6)$$

$$4UO_2 + 3ThCl_4 + Th = 4UCl_3 + 4ThO_2 \quad (2.7)$$

$$4U_3O_8 + 9ZrCl_4 + 7Zr = 12UCl_3 + 16ZrO_2 \quad (2.8)$$

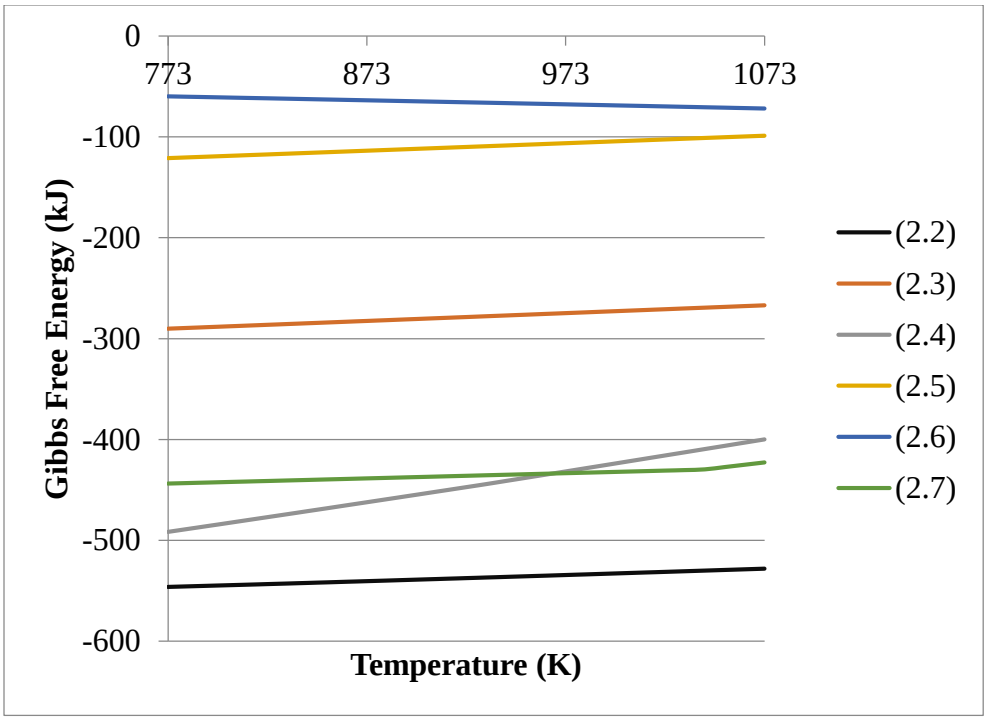

Figure 2.2 Calculated free energy change for reaction of UO_2 with various chlorides to form UCl_3. HSC Chemistry 7.1 was used for these calculations.

$$4U_3O_8 + 9TiCl_4 + 23Ti = 12UCl_3 + 32TiO \quad (2.9)$$

$$3U_3O_8 + 9AlCl_3 + 7Al = 9UCl_3 + 8Al_2O_3 \quad (2.10)$$

$$2U_3O_8 + 3WCl_6 + 5W = 6UCl_3 + 8WO_2 \quad (2.11)$$

$$3U_3O_8 + 9VCl_3 + 7V = 9UCl_3 + 8V_2O_3 \quad (2.12)$$

$$4U_3O_8 + 9ThCl_4 + 7Th = 12UCl_3 + 18ThO_2 \quad (2.13)$$

$$4PuO_2 + 3ZrCl_4 + Zr = 4PuCl_3 + 4ZrO_2 \quad (2.14)$$

$$4PuO_2 + 3TiCl_4 + 5Ti = 4PuCl_3 + 8TiO \quad (2.15)$$

$$3PuO_2 + 3AlCl_3 + Al = 3PuCl_3 + 2Al_2O_3 \quad (2.16)$$

$$2PuO_2 + WCl_6 + W = 2PuCl_3 + 2WO_2 \quad (2.17)$$

$$3PuO_2 + 3VCl_3 + V = 3PuCl_3 + 2V_2O_3 \quad (2.18)$$

$$4PuO_2 + 3ThCl_4 + Th = 4PuCl_3 + 4ThO_2 \quad (2.19)$$

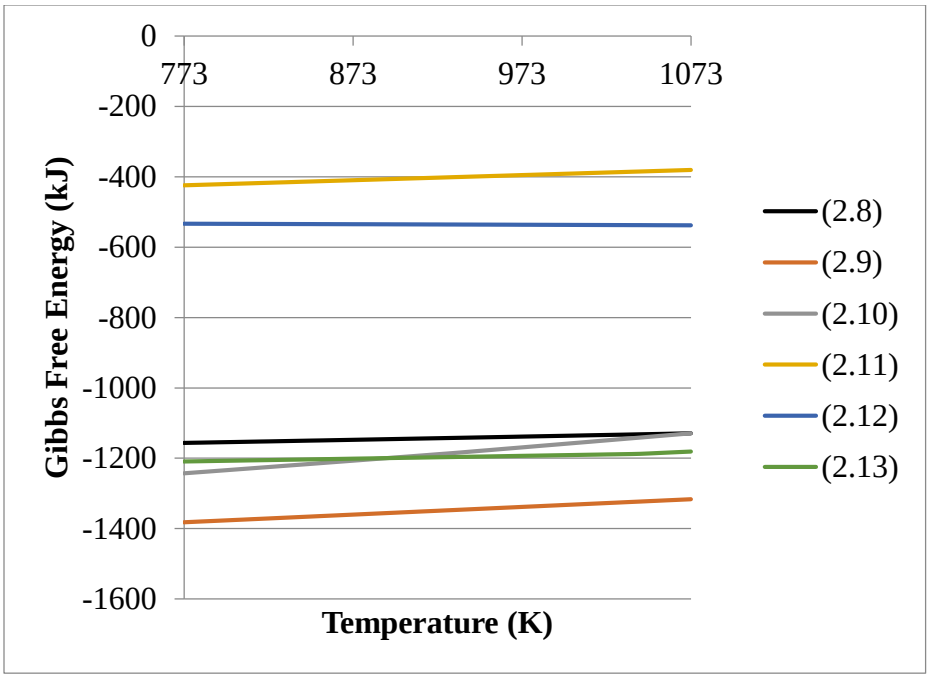

Figure 2.3 Calculated free energy change for reaction of U_3O_8 with various chlorides to form UCl_3. HSC Chemistry 7.1 was used for these calculations.

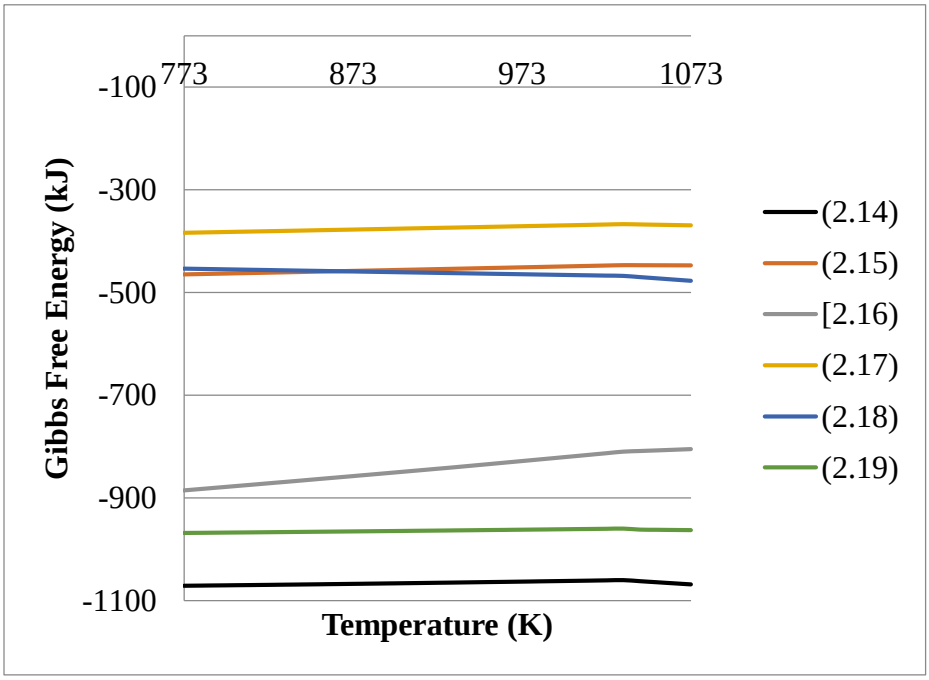

Figure 2.4 Calculated free energy change for reaction of PuO_2 with various chlorides to form $PuCl_3$. HSC Chemistry 7.1 was used for these calculations.

2.4 Conclusions

Clearly, there are a number of credible diversion scenarios for pyroprocessing, which motivates the development of safeguards technology. A wide range of technology options are being researched to mitigate the proliferation risk. A chlorination diversion scenario in which actinides are partitioned from the fuel basket to the salt in the DER process is of particular concern, since it has not been widely recognized. This thesis reports further investigation into the threat of this diversion scenario and how it might be detected in a declared commercial facility.

CHAPTER 3

ABSORPTION SPECTROSCOPY LITERATURE REVIEW

Absorption spectroscopy, as mentioned in Chapter 2, is one of the viable technologies for monitoring the composition of the molten salt used in the oxide reduction process. This chapter reviews the literature and state of the art for absorption spectroscopy applied to analysis of molten salts.

Pioneering work in optical absorption spectroscopy of high temperature molten salt was conducted during the late 1950s and 1960s.[13] More recently, ultraviolet and visible (UV-vis) spectroscopy experiments of various molten salt systems have been performed. UV-vis spectroscopy work related to pyroprocessing has been published on the following salt systems: NaCl-KCl[13] LiCl-KCl[37], LiCl[15], NaCl-2CsCl[15], CsCl[15], $CaCl_2$[15], LiCl-$SrCl_2$[16], CsCl-$SrCl_2$,[16] and LiF-NaF-KF.[38]

UV-Vis spectroscopy is an optical absorption spectroscopic technique. UV-Vis spectroscopy is based on absorption which measure transitions from the ground state to the excited electron state of atoms. Each chemical species has a unique electronic configuration, which is excited by particular wavelengths of light. Equation 2.1 is used to measure absorbance in intensities of incident light and transmitted light. Furthermore, this can be measured as a function of time in the wavelength range between 300 and 1000 nm.

Resulting absorption spectra would contain peaks associated with the electronic transition between high electron orbital states within various elements. The amplitude of the absorption peak is related to the concentration of elements and is given by:

$$A = \varepsilon c d \tag{3.1}$$

where ε is molar absorptivity or extinction coefficient, c is molar concentration, and d is the path length of light through absorbing media, which is equal to the thickness of the optical cell. Consequently, when a known spectrum of light is directed through a sample, the species present and their concentration can be deduced.

Tables 3.1, 3.2, and 3.3 summarize all the species that have been studied to date by UV-Vis spectroscopy in molten salts. Spectroscopy has been utilized for a number of fundamental studies of ion structure in molten choride salts. Fukasawa et al. showed that the octahedral structure of Nd(III) ions in LiCl was stabilized by the addition of alkali (NaCl, KCl, RbCl, or CsCl)[2] and alkaline ($CaCl_2$, $SrCl_2$, or $BaCl_2$)[39] salts. The Nd(III) complex was more stable in chloride mixtures with larger averaged cationic radii. These results correlate with the polarizing power of solvent cations. The results suggested that the octahedral symmetry of the $NdCl_6^{3-}$ complex was more distorted in melts with higher LiCl content, and the distortion was depressed by decreasing the polarizing power of solvent cations. Also, the local structure around Nd^{3+} was significantly correlated with the thermodynamic stability of the Nd(III) complex in molten chlorides. Temperature was also shown to affect structure of various species within molten salts. Higher temperatures were found to increase the intensity of the spectrum lines.

Table 3.1: Major absorption peaks of transition metal ions in various molten salts.

Cation	Base Salt	Absorption Bands (nm)
Ti(III)[42]	LiCl-KCl	769, 1000
V(IV)[42,43]	LiCl-KCl	720
V(II)[42,43]	LiCl-KCl	550
V(III)[42,43]	LiCl-KCl	555, 911
V(IV)[42,43]	LiCl-KCl	717
Cr(II)[42]	LiCl-KCl	1020
Cr(III)[42]	LiCl-KCl	540, 800
Fe(II)[42]	LiCl-KCl	2083
Co(III)[44]	NaCl-KCl	608
Co(II)[42,44]	NaCl-KCl	608
Co(II)[42,44]	LiCl	600
Co(III)[42]	LiCl-KCl	610, 670, 710
Ni(II)[42]	LiCl-KCl	260
Cu(II)[42]	NaCl-KCl	320
Mo(III)[45]	LiCl-KCl	425, 552, 685
Pd(II)[46]	LiCl-KCl	500

Composition of various lithium chloride binary salts has been shown to be quantifiable by UV-Vis spectroscopy. A number of researchers have produced linear calibration curves for specific spectrum peaks for various ionic species. Park et al. performed spectroscopy on a LiCl-KCl-UCl_3 melt and obtained U calibration curves showing a good linearity up to concentration levels of 0.15%.[29] This is a promising finding with respect to applying UV-Vis spectroscopy to the detection of diversion scenarios involving chlorination of actinides into the molten salt used for oxide reduction. In normal

Table 3.2: Major absorption peaks of rare earth ions in various molten salts.

Cation	Base Salt	Absorption Bands (nm)
Ce(III)[47]	LiCl-KCl	317, 340
Pr(III)[48,49]	LiCl-KCl	450, 487
Pr(III)[48]	NaCl-CsCl	450, 487
Pr(III)[48]	LiCl	487
Pr(III)[48]	$CaCl_2$	486
Nd(III)[37,49,50]	LiCl-KCl	589, 740, 804
Nd(III)[37,50]	LiCl	585
Nd(III)[39]	LiCl-$CaCl_2$	585
Nd(III)[39]	LiCl-$SrCl_2$	585
Nd(III)[39]	LiCl-$BaCl_2$	585
Nd(III)[50]	LiCl-NaCl	589
Nd(III)[50]	LiCl-CsCl	589
Sm(III)[49,51]	LiCl-KCl	2000
Sm(II)[51,52]	LiCl-KCl	260
Eu(III) [53]	LiCl	305
Eu(II)[53]	LiCl	350
Dy(III)[51]	LiCl-KCl	301, 352, 389, 454, 1300
Dy(III)[51]	LiCl-CsCl	1300
Ho(III)[51]	NaCl-CsCl	451, 459
Ho(III)[51]	LiCl-CsCl	451, 460
Ho(III)[49,51]	LiCl-KCl	451, 460
Er(III)[51]	NaCl-CsCl	377
Er(III)[51]	LiCl-CsCl	377
Er(III)[49,51]	LiCl-KCl	377

Table 3.3: Major absorption peaks of actinide ions in various molten salts.

Cation	Base Salt	Absorption Bands (nm)
U(II)[42]	LiCl-KCl	260
U(III)[29,30,40,41,42,54,55]	LiCl-KCl	453, 551, 898, 1050
U(IV)[56]	LiCl-$SrCl_2$	1141
U(IV)[56]	CsCl-$SrCl_2$	1110
Np(III)[54]	LiCl-KCl	560
Np(IV)[54]	LiCl-KCl	530, 585, 665, 740, 837
Np(V)[54,57]	LiCl-KCl	990
Pu(III)[58]	LiCl-CsCl	580, 1410
Pu(IV)[58]	LiCl-CsCl	680, 890, 1130
Pu(V)[58]	LiCl-CsCl	900
Pu(VI)[58]	LiCl-CsCl	600, 1000
Pu(VI)[57]	$LiNO_3$-KNO_3	830
Am(III)[57]	$LiNO_3$-KNO_3	510, 800

operations, there would be no detectable amount of actinides in the salt. If UV-vis can detect low concentrations as demonstrated by Park, it could be an effective method to be used by inspectors. The minimum detectable concentrations obtained with a confidence level of 99% were found to be 5.83×10^{-4}, 2.39×10^{-4}, and 3.90×10^{-3} wt.% for absorption peaks at 453 nm, 551 nm, and 898 nm, respectively. Further work showed a U calibration curve with good linearity up to a concentration of 13.6 wt%, indicating that UV-vis spectroscopy may also be useful for NMA measurements. One important concern, however, is the potential interference of other species in the salt. The ER salt, in particular, is loaded with a wide spectrum of metal chlorides. The most complex composition analysis

by UV-vis spectroscopy appears to have been performed by Fujii et al.[30] LiCl-KCl eutectic melts containing concentrations of RE and U closely matching spent nuclear fuel cooled for 4 years from a 152.4 GW d/t fast breeder reactor were examined. This demonstrated the feasibility of distinguishing and quantifying various species in complex salt mixtures. Based on the spectral data, the U concentration was measurabe within 1% analytical uncertainty.

Moving towards the goal of live online monitoring, several papers have been published on spectral change during chemical and electrochemical reactions. Kim et al. monitored the spontaneous reduction of Eu(III) to Eu(II) as well as after performing cyclic voltammetry.[21] Park et al. demonstrated live absorption spectroscopy during chronopotentiometry.[29] Another paper by this group showed the real-time monitoring of the U(III) to U(IV) reduction process in LiCl-KCl eutectic melt.[40] Addition of Li_2O and Nd_2O_3 into a LiCl-KCl-UCl_3 melt was also monitored live by the aforementioned group.[41] Significant spectral changes were observed from the addition of oxide and lanthanide ions to the melt.

Overall, these past studies have primarily focused on rare earth elements (RE) and uranium in binary molten chlorides. For the most part, the analysis of RE accumulation is only relevant to electrorefining salts. RE do not form soluble salts in the LiCl-Li_2O used for oxide reduction under normal operating conditions, and thus are unlikely to interfere with actinide detection in the OR process. On the other hand, the accumulation of Group I and II fission products (Cs, Sr, Ba, and Rb) does occur during OR operation. Potential interference by these species, thus, needs to be understood.

Another key application of online monitoring for electrolytic reduction is control

of Li_2O concentration in the electrolyte. It has been found that Li_2O is typically consumed by each batch of oxide fuel that is reduced. In typical OR operation, samples of the salt are taken and subjected to a titration in water to calculate Li_2O concentration. This analysis can be performed in a shielded air-atmosphere hot cell—either collocated with the process or in a dedicated analytical chemistry facility. There is the potential to also use spectroscopy for this analysis, which could yield results more quickly. This type of testing would likely be useful for IAEA inspectors visiting the pyroprocessing facility. An inspector could have salt samples randomly taken from virtually any step in the flowsheet and rapidly analyzed using a secure optical spectroscopy instrument within the hot cell. The testing would indicate if diversion or suspicious activity has taken place during oxide reduction and/or electrorefining.

CHAPTER 4

MOLTEN SALT ELECTROCHEMISTRY

4.1 Introduction

Molten salt electrochemistry, as mentioned in Chapter 2, is one of the viable technologies for monitoring the composition of the molten salt used in the oxide reduction process. This chapter reviews the literature and state of the art for electrochemistry applied to analysis of molten salts.

Molten salt electrochemistry dates back to 1802 when Sir Humphrey Davy described electrochemistry experiments in KOH and NaOH. Around 1930, molten salt was put to use in nuclear applications by Westinghouse Lamp Company.[59] Molten salts are conducive to wide range of electrochemical applications, such as electrowinning, electrodeposition, and energy storage. A major benefit of halide molten salt systems is their high boiling point, high solubility for actinide halides, high electrical conductivity, and wide electrochemical window. Unlike aqueous-based electrochemistry, which has narrow potential window (0.0V to -1.23 V), molten salts have wide potential windows. Generally, the accessible potential range is between halogen gas evolution (anodic limit) and alkali metal deposition (cathodic limit). In the case of LiCl, the anodic and cathodic limits are Cl_2 evolution and Li deposition, respectively, which represents an accessible potential range

of 3.47 V at 923 K. Since molten salts have high boiling points, thermodynamics of a molten salt process can be controlled with the adjustment of the melt temperature. Several electrochemical analytical techniques can be used to qualitatively and quantitatively monitor molten salt pools during pyroprocessing. Direct electrolytic reduction (DER) salt is especially amenable to electrochemical-based monitoring owing to its uncomplicated composition. DER salt if used properly will contain fission products and no actinides or lanthanides. DER processing of oxide fuel results in the diffusion of Cs, Ba, Sr, and Rb into the LiCl-Li_2O processing salt. By monitoring for the presence of actinides and lanthanides, an inspecting agency could easily detect misuse.

4.2 Electrochemistry Theory

Electrochemistry is concerned with studied the electric charge transfer capabilities of an electrochemical cell through an ionic solution. A basic electrochemical cell consists of two half-cells, which can further be subdivided into electrode and electrolyte components. The standard potential of the electrochemical cell is the overall voltage between the cathodic and anodic components of a cell. The two electrodes of electrochemical cell are the cathode and anode. Reduction of oxidized species occurs at the cathode and oxidation of reduced species occurs at the anode. This redox reaction occurs simultaneously at both electrode is an electrochemical cell and can be written as follows:

$$O + ne^{-} \rightleftarrows R \tag{4.1}$$

where O is the oxidized species, R is the reduced species, and n is number of electrons transferred in the redox reaction. Applying a three-electrode system coupled with a potentiostat allows for the control of the redox reactions occurring in cell. With the use of a potentiostat, the occurrence of an oxidation or reduction reaction is controlled based on applied potential at a working electrode. A working electrode acts as an anode or cathode depending on the applied potential and a counter electrode finish out the circuit. To measure both the potential and current in the cell, a reference electrode, with a constant composition, is used.

Cyclic voltammetry (CV) is a common electrochemical where a potential is ramped at a constant scan rate between two vertex potentials. This potential change allows for the measure of both reduction and oxidation. An upsurge in current occurs at given potential depending on the number and rate of electrons transferred. This potential sweep method can be used to diagnose electrochemical reaction mechanisms, identify electroactive species present, and indicate relative concentrations of ionic species by resulting current response. More broadly, most electrochemical studies start with CV work to find the potential region in which there is electrodic activity. The Berzins-Delahay equation is applied to CV data for analysis of charge transfer, diffusion, and concentration if the system is reversible [60].

$$i_p = 0.6105\left(\frac{F^3}{RT}\right)^{1/2} n^{3/2} A D^{1/2} C v^{1/2} \quad (4.2)$$

where i_p is the peak current, F is the Faraday constant, R is the universal gas constant, T is the temperature in Kelvin, n is the number of electrons transferred, C is the concentration

of the analyte in the bulk solution, A is electrode area, D is the diffusion coefficient, and ν is scan rate. Fundamentally, an electrochemical cell is considered reversible if no side products or no new reactions occur when the cell current is reversed. Based on CV data, reversibility is shown if the peaks do not shift with ν, $I_{p,c}$ or $I_{p,a} \sim \nu^{1/2}$ or $I_{p,c} = I_{p,a}$. Furthermore, using the cathodic potential peak, the reversibility of the redox reaction is determinable.

Chronoamperometry (CA) is a potentiostatic technique based on the principle that when an electroactive species is oxidized or reduced at an electrode, the resulting current is proportional to the concentration of the species. Unlike voltammetric methods where the working electrode is scanned between selected potentials with current response measured, in CA, the potential is changed instantaneously and a current-time curve is recorded. CA is useful for obtaining diffusion coefficients, adsorption parameters, rates of coupled chemical reactions, and rates of electron transfer process. In cases of diffusion control of the electrode process, the Cottrell equation can be applied.[60]

$$i(t) = nFA\sqrt{\frac{D}{\pi}}C^o \tag{4.3}$$

where i(t) is current with respect to time, n is the number of electrons transferred, F is Faraday constants, A is the area of the working electrode, D is the diffusion coefficient, and C^o is the initial concentration. If $i=f(t^{-1/2})$ is linear than the process is diffusion controlled.

4.3 Application of Molten Salt Electrochemistry to Actinide Measurement

An understanding of actinide electrochemistry in molten salts is critical in the development and commercialization of preprocessing. Thorium, protactinium, uranium, neptunium, plutonium, americium and curium have all been studied electrochemical in halide molten salts.[61] Of particular interest for international safeguarding is the electrochemical behavior of uranium and plutonium in pyroprocessing molten salt pools. Literature shows that actinide standard potentials decrease with increase in molten salt temperature. Uranium has been report stable as U^{3+}, U^{4+}, and U^{6+} oxidation states in LiCl-KCl. The apparent standard potential of U^{3+}/U^0 has been found to be 2.46 V at 823 K and a fitted correlation has been reported for temperatures range 673 - 823 K:[61]

$$E^*_{U^{3+}/U} = -2.9429 + 5.8724 \times 10^{-4}T \tag{4.4}$$

Kuznetsov et al. reported diffusion correlation for U^{3+} valid from 723 to 823K:[62]

$$D_{UCl_3}(cm^2/s) = 2.291 \times 10^{-3} \exp\left(-\frac{32550}{RT}\right) \tag{4.5}$$

This diffusion correlation is in good agreement with literature values reported. U^{4+} is another stable ion of uranium that has been reported present in LiCl-KCl. U^{4+} reduces to U^0 in two steps:

$$(1)\ U^{4+} + e \rightarrow U^{3+} \tag{4.6}$$

$$(2)\ U^{3+} + 3e \rightarrow U^0 \tag{4.7}$$

Between 723 and 823 K, an apparent standard potential for U^{4+}/U^{3+} has been reported as:[61]

$$E^{*}{}_{U^{4+}/U^{3+}} = -1.669 + 2.1 \times 10^{-4}T \quad (4.8)$$

Kuznetsov et al. reported diffusion correlation for U^{4+} valid from 723 to 823K:[62]

$$D_{UCl_4}(cm^2/s) = 3.467 \times 10^{-3} \exp\left(-\frac{37450}{RT}\right) \quad (4.9)$$

As discussed above, there is an abundance of data on actinide electrochemistry in LiCl-KCl. However, there is no literature data available on the electrochemistry of actinides in LiCl salt. Moreover, there is no literature on measurement of actinide concentrations in DER salt (LiCl). This is a major knowledge gap that needs to be filled, especially for safeguarding of oxide fuel pyroprocessing.

CHAPTER 5

EXPERIMENTAL METHODS

5.1 Methods

In this chapter, details of the new experiments performed for this study are presented. The approach was to first experimentally simulate the chlorination reaction as a potential diversion scenario in the direct electrolytic reduction (DER) process. Then several promising monitoring approaches were tested on the salts—including voltammetry, thermal analysis, and UV-vis spectroscopy.

5.2 Materials

Lithium chloride was procured from Alfa Aesar as anhydrous with a purity of 99.9%. However, moisture was observed emanating from this salt and coating the upper section of the quartz cuvettes during preliminary UV-Vis spectroscopy experiments. This moisture is believed to have contributed to cracking of the cuvettes during the ramp up to 923K. To remedy this problem, LiCl was dried in a muffle furnace by following an unpublished procedure (Table 5.1) used at Chungbuk National University by Prof. Sang Mun Jeong. LiCl salt within Pyrex beakers was heated systematically in a muffle furnace (Lindberg Blue M, Thermo Scientific) in open atmosphere. Immediately after completion of the drying process, the beakers of salt were transferred into the glovebox. After drying,

Table 5.1: Heating scheme for drying LiCl salt in a muffle furnace in open atmosphere.

Temperature (K)	**Time (hr)**	**Segment**
393	0.33	Ramp
393	3	Hold
523	15	Ramp
523	5	Hold
723	15	Ramp
723	2	Hold
473	3	Ramp
473	24	Hold

moisture was not observed during UV-Vis spectroscopy. This dried LiCl was used in all further experimental work.

Cesium chloride with a purity of 99.9% and strontium chloride with a purity of 99.5% were procured from Alfa Aesar. Cesium chloride and strontium chloride make up a significant portion of the fission products that diffuses into direct electrolytic reduction (DER) salt. These salts were added to investigate their effect on the spectral and electrochemical properties during various experiments. Zirconium tetrachloride (99.5%, Alfa Aesar) was chosen as the chlorinating agents for uranium oxide (U_3O_8, New Brunswick Laboratory) and neodymium oxide (99.99%, Alfa Aesar). Zirconium foil (99.8%, Strem) was also used during the chlorination experiments.

5.2.1 Spectroscopy Salt Preparation Procedure

Powder chemicals tend to stick to quartz tube walls and cause inaccurate composition of salt melt. To remedy this, a homogenization/granulation process was undertaken. Initially, all salts are premixed in an alumina crucible. Salt mixture is homogenized by melt in Kerr Auto Electro-Melt Furnace. The melt is heated to 923K and

poured while molten into a clean stainless steel pan. This forms large solid salt pieces. Afterwards, the particle size is reduced.

5.3 Equipment and Procedures

5.3.1 Glovebox

The hygroscopic nature of LiCl and other chloride salts used necessitates that experimental work be conducted in a dry and inert environment. All electrochemical and spectroscopy experiments were conducted in argon atmosphere within an Innovative Technology PureLab HE glovebox, shown in Figure 5.1. The H_2O and O_2 content were maintained below 0.5 ppm for all experiments.

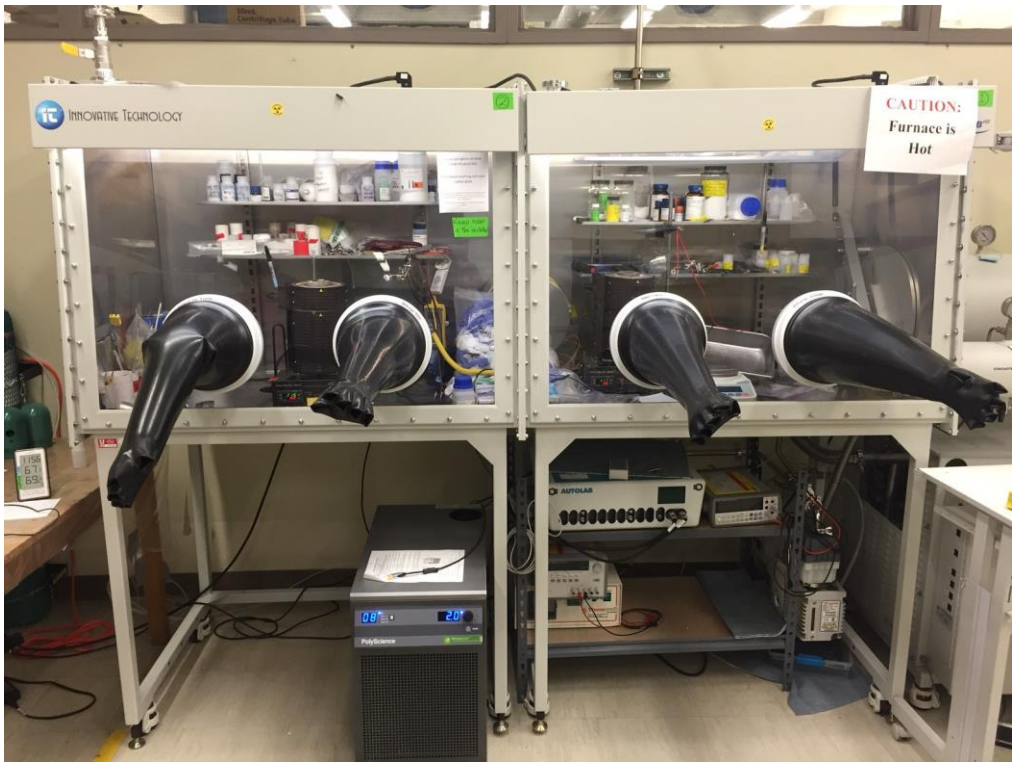

Figure 5.1: Argon atmosphere glovebox. Moisture and oxygen were keep below 0.5 ppm for all experiments within the glovebox.

5.3.2 Chlorination Procedure

The objective of chlorination was to simulate a diversion scenario involving the DER process. All reactions were performed in molten LiCl with 1 wt% CsCl and 1 wt% $SrCl_2$. The reactions that were attempted were as follows:

$$4U_3O_8 + 9ZrCl_4 + 7Zr = 12UCl_3 + 16ZrO_2 \quad (5.1)$$

$$Nd_2O_3 + 3/2\ ZrCl_4 = 2NdCl_3 + 3/2\ ZrO_2 \quad (5.2)$$

Initially, the objective was to load the LiCl with a significant amount of $ZrCl_4$.

Because $ZrCl_4$ is volatile at the DER reaction temperature (923 K), it is necessary to follow a special procedure to trap it in the salt before it all vaporizes. A trapping method was attempted for adding 99.5% $ZrCl_4$ (Alfa Aesar) to LiCl with 1 wt% $SrCl_2$ (99.5%, Alfa Aesar) and 1 wt.% CsCl (99.9% Alfa Aesar). A LiCl-$SrCl_2$–CsCl ingot was formed within a tapered glassy carbon crucible (Sigraur GAT 19, HTW Hochtemperatur-Werkstoffe GmbH). The bottom of the ingot was cut off. Into the bottom of the glassy carbon crucible $ZrCl_4$ was added and atop the cut ingot was place. Figure 5.2 depicts the setup. The setup was heated to 923 K in a Kerr furnace. This trapping method was shown by previous researcher to minimize the escape of sublimed $ZrCl_4$, which sublimates at 604 K, in LiCl-KCl eutectic.[63] However, as will be discussed in the results section, that method proved ineffective.

A sintered UO_2 pellet was dropped in molten post trapping method salt. After allowing the UO_2 pellet to equilibrate with the molten salt for an hour, Zr foil was suspended in the salt. The Zr foil reacted with the salt for one hour and electrochemical

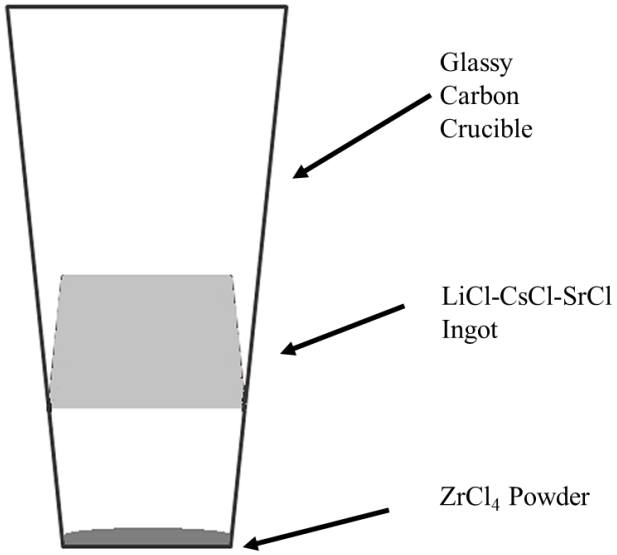

Figure 5.2: Schematic of $ZrCl_4$ addition to LiCl-$SrCl_2$-CsCl via trapping method.

tests were performed. A second chlorination run was performed by lowering $ZrCl_4$ within a stainless steel cup in combination with a suspended 0.25 mm thick 99.8% Zr foil (Strem) into the molten LiCl based salt. Figure 5.3 depicts the first and second chlorination setups. The addition of Zr foil suppressed the loss of zirconium chloride by converting zirconium tetrachloride to a tri and dichloride. Oxides on the Zr foil surface were removed grinding the surface with a small handheld power drill with a metal brush attachment prior to use for chlorination. The grinding was done within the glovebox.

In the chlorination of UO_2-Nd_2O_3 pellet, the second chlorination methodology employed in UO_2 chlorination was used right away. A sinter UO_2-Nd_2O_3 pellet was dropped into molten LiCl- 1 wt% $SrCl_2$- 1 wt% CsCl salt. After allowing the UO_2-Nd_2O_3 pellet to equilibrate with the molten salt for an hour, $ZrCl_4$ and Zr were added to the salt. $ZrCl_4$ was added within a stainless steel dipping cup in combination with Zr foil into the molten LiCl based salt. The reaction was allowed to proceed for an hour before the stainless steel cup

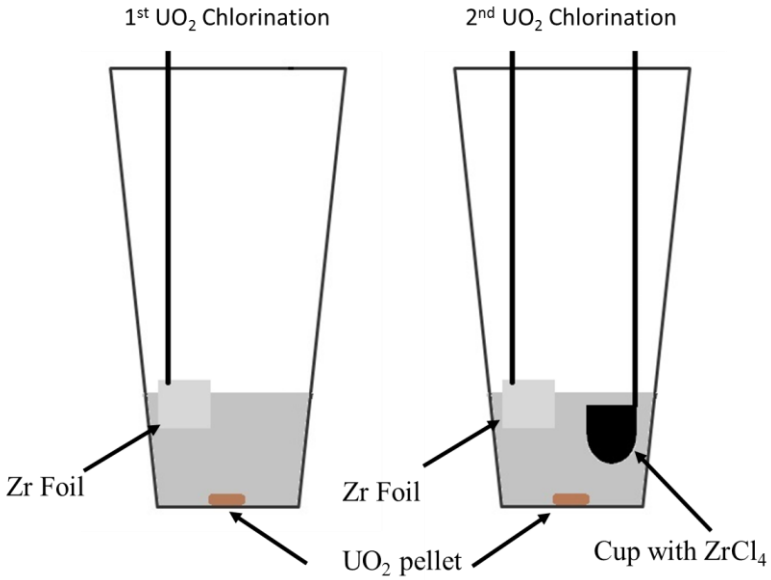

Figure 5.3: Schematic of two stages chlorination of UO_2 in LiCl-$SrCl_2$–CsCl-$ZrCl_{4-x}$ salt at 923 K.

and Zr foil were removed from the salt. Figure 5.4 shows an image of the stainless steel cup and Zr foil after one hour of submersion in molten salt.

5.3.3 Pelletization Procedure

To introduce uranium oxide in LiCl-based salt without having it disperse and float through in the salt, U_3O_8 (natural uranium, New Brunswick Laboratory) was pelletized. Zinc stearate (technical grade, Aldrich) was mixed in with U_3O_8 as a binding agent in five to ninety-five ratio. This mixture was introduced into a die set and pressed in 15-ton laboratory manual pressing machine (LPM-15T, Col-Int Tech). Subsequently, the resulting pellet was sintered in a compact muffle furnace (KSL-1100X-S, MTI Corporation) that was ramped at 300 K/h to 1373 K and held there four hours. The pellet was allowed to cool naturally within the muffle furnace. The zinc stearate and oxygen evolved off during

Figure 5.4: Image of stainless steel cup and Zr foil after one hour of submersion in molten salt at 923 K.

sintering, and the resulting pellet was a black-brown color. The same procedure was followed when preparing a pellet originally contenting 90 wt% U_3O_8 10 wt% Nd_2O_3 (99.99%, Alfa Aesar). Figure 5.5 shows a UO_2-Nd_2O_3 pellet after sintering within the argon filled glovebox.

5.3.4 UV-Vis Spectroscopy Equipment and Procedure

Figure 5.6 shows a schematic of the UV-Vis molten salt spectroscopy setup. A UV quartz cuvette (T1GS-Q-10, REFLEX Analytical Corp.) with extended graded seal was used. The cuvette had a 10 mm path length. Approximately 6 grams of salt are added to a UV-Vis cuvette. The cuvette is secured in custom alumina furnace lid. The cuvette is slowly heated for three hours at approximately 5 K min^{-1} to 923 K in a vertical solid tube furnace (Thermcraft Inc.) The furnace has optical ports for light to pass through. A deuterium and halogen light source (DH 2000, Ocean Optics), which is warmed up for 40

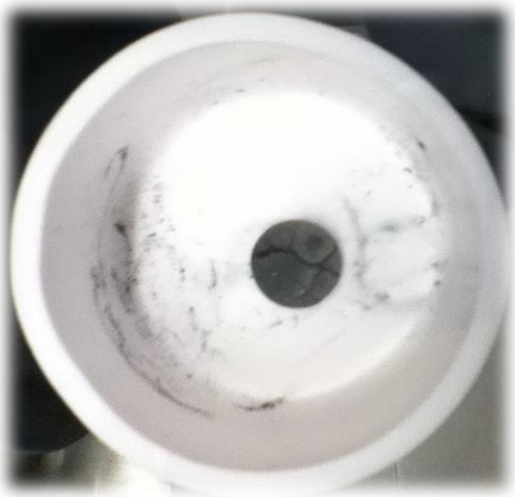

Figure 5.5: UO_2-Nd_2O_3 pellet after sintering.

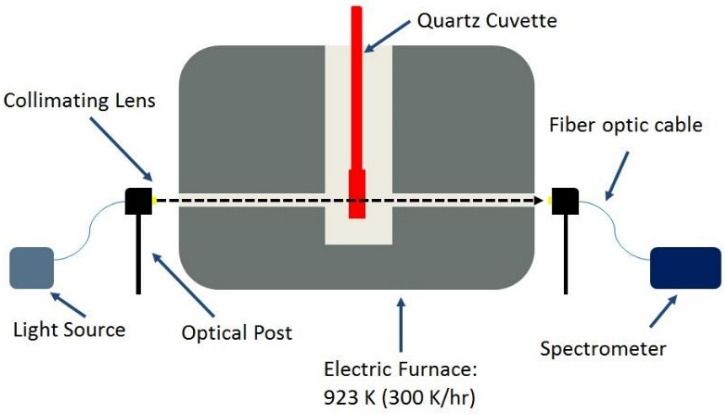

Figure 5.6: Schematic of UV-Vis spectroscopy experimental setup. All experiments were conducting within a glovebox in an argon environment.

minutes to obtain a steady UV-Vis light spectrum, is used. Solorization-resistant fiber optic cables (QP400-SR, Ocean Optics) guide the light in and out the optical ports. The outlet light is captured in a collimating lens (84-UV-25, Ocean Optics) and fed into a modular spectrometer (QE65 Pro, Ocean Optics). Finally, the spectral data are captured and processed in Oceanview software (Ocean Optics). Quartz cuvettes crack during solidification of the salt thus are not reusable.

5.3.5 Electrochemical Test Assembly and Procedure

All electrochemical tests were performed in a Kerr Electro Melt furnace with a removable graphite inner liner. The alumina fiber furnace lid had 50 mm diameter hole through which an electrode assembly could be place or reagents could be added to a melt. The furnace has a maximum operational temperature of 1393 K. The graphite inner liner allowed the use of a crucibles up to 60 mm in diameter. Figure 5.7 shows the Kerr furnace operating with an electrode assemby in the glovebox.

The working and reference electrodes were situated near each other. If the counter and working electrode are situated too closely, reactions occurring at the counter electrode

Figure 5.7: Kerr furnace operating within the glovebox.

may interfere with those occurring at the working electrode. Autolab potentionstat (PGSTAT128N, Metrohm) was used. The reference electrode Ag/AgCl contained within a 10 mm inner-diameter quartz tube with a thinned bottom. The base salt, LiCl, was premixed with 1 mol% AgCl (99.9%, Alfa Aesar). The working electrode consisted of an alumina sheathed 0.5 mm 99.95% W wire (Alfa Aeser). The counter electrode consisted of an alumina sheathed 0.5 mm 99.95% Pt wire (Alfa Aesar). The electrode details are summarized in Table 5.2.

Electrochemical experiments were performed within an alumina crucible (AL-1250, AdValue Tech) heated in a Kerr Auto Electro-Melt Furnace. A graphite inner liner was used to protect the heating elements of the furnace in case of crucible breakage. Salts were heated at 240 K/h to 923 K. Owing to thermal shock sensitivity, the reference electrode was preheated slowly above the melt. Once the melt reach 923 K, the reference electrode was slowly lowered into the melt. The working and counter electrodes were lowered into the melt once the reference electrode was ready. The counter electrode area was 7-10 times larger than the working electrode area to minimize diffusion limitations. A schematic of the electrochemical experimentation setup is shown in Figure 5.8.

Table 5.2: Electrodes using for cyclic voltammetry of molten LiCl salts.

Electrode	**Material**
Working Electrode (WE)	0.5 mm 99.95% Tungsten wire
Reference Electrode (RE)	0.5 mm 99.9% Silver wire in 1 mol% AgCl in LiCl
Counter Electrode (CE)	0.5 mm 99.95% Platinum wire

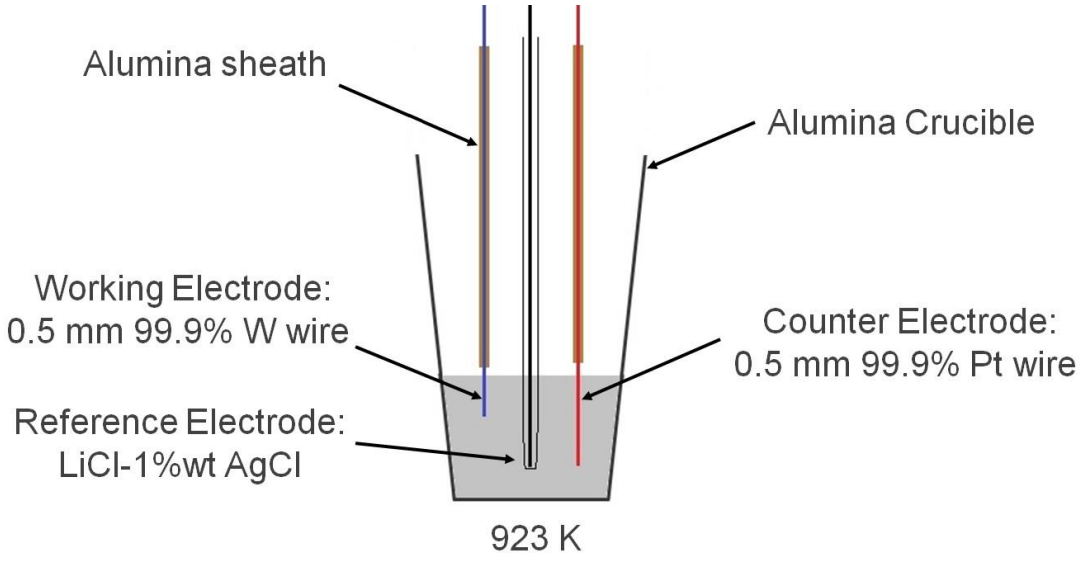

Figure 5.8: Schematic of electrochemical experimental setup. All experiments were run in an argon environment within a glovebox.

5.3.6 Differential Scanning Calorimetry Equipment and Procedure

To measure temperature-induced changes in the salt such as phase transformations and dehydration, a TGA/DSC unit (SDT Q600, TA Instruments) was used. Figure 5.9 shows an image of the TGA/DSC unit. Samples of 10-20 mg salt were prepared within the glovebox and placed in a Pt pan. Subsequently, small glass vials were utilized to transport the salt filled pan out of the glovebox. The pans were carefully removed from the glass vials, placed on the Q600 sample stage, and the temperature cycle was started. A continuous flow of ultra-high purity argon (100 ml/min) was flowed over the samples during operation. A ramp up at 10 K/min to 923 K was followed by a ramp down at 10 K/min. The mass changes and heat flow relative to an empty Pt pan were recorded. After each run, the salt was rinsed out of the pan using nanopure DI water. Afterwards, the Pt pan was dried at 423 K prior to being reused.

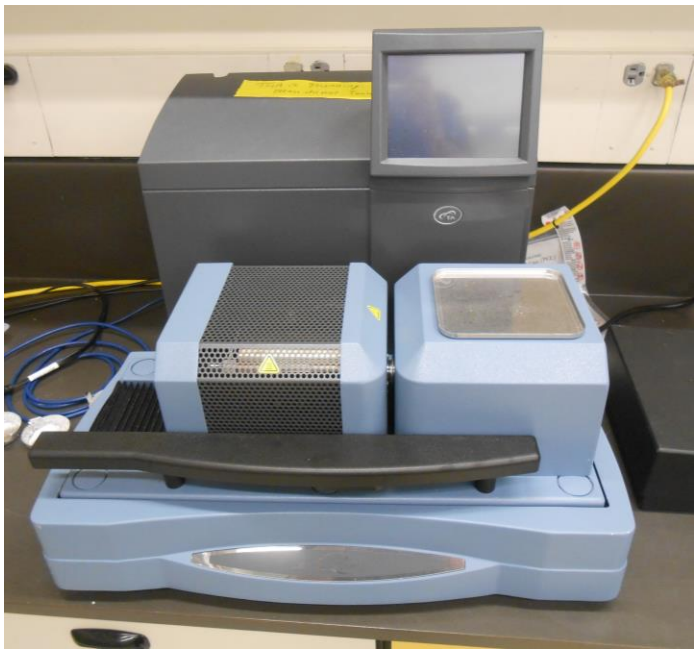

Figure 5.9: The DSC/TGA unit used for thermal analysis of salt samples. Samples were run to 923 K under the flow of ultrapure argon.

CHAPTER 6

RESULTS AND DISCUSSION

6.1 Introduction

A series of experiments were undertaken to find a potentially suitable method for safeguard monitoring of oxide reduction (DER) process. The possibility of diverting actinides into the DER salt was investigated by electrochemical, calorimetric, and optical spectroscopic methods. Images of salt ingot at various stages of experimentation are shown in Figure 6.1. Figure 6.1(a) shows LiCl- 1 wt% $SrCl_2$- 1 wt% CsCl salt ingot which is a bright white color. Figure 6.1(b) shows a salt ingot after reaction of LiCl- 1 wt% $SrCl_2$- 1 wt% CsCl with $ZrCl_4$ powder and Zr foil; the salt turns a light brown color. Figure 6.1(c) shows the LiCl-$SrCl_2$-CsCl-$ZrCl_{4-x}$ salt after chlorination of uranium oxide; the salt ingot turns a black color with slight red hue.

6.2 Electrochemistry

Table 6.1 summaries the calculated free energies of formation and standard reduction potential for chloride salts present in this study. Cyclic voltammograms were recorded for LiCl-1 wt% $SrCl_2$-1 wt% CsCl, the same salt post chlorination of UO_2, and that same salt post chlorination of UO_2/Nd_2O_3. Figure 6.2 shows the results for the base

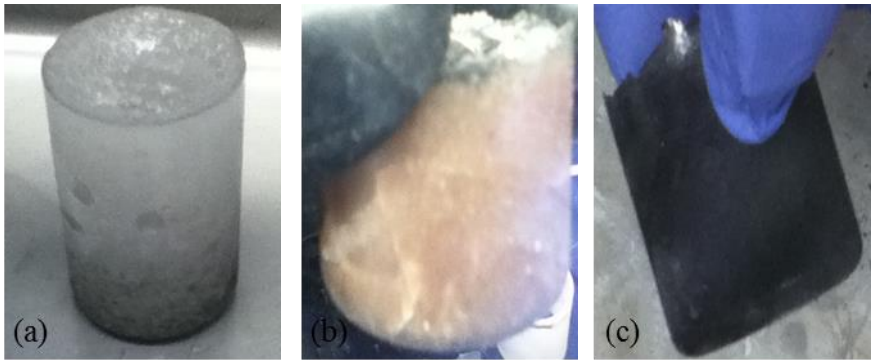

Figure 6.1: Images of salt ingot following electrochemical experiments: (a) LiCl-1 wt% $SrCl_2$- 1wt% CsCl (b) LiCl-$SrCl_2$-CsCl-$ZrCl_{4-x}$ (c) LiCl-$SrCl_2$-CsCl-UCl_3

Table 6.1: Free energies of formation and standard reduction potentials for chloride salts present in this study. Free energies of formation at 923 K. Calculated standard reduction potential at 923 K in relative to Ag/(1 wt% AgCl).

Reagent	**ΔG_f (kJ/mol)**	**E^o vs. Ag/1 wt% AgCl (V)**
LiCl	-485.836	-2.3762
CsCl	-559.624	-2.6013
$SrCl_2$	-973.536	-2.4522
$ZrCl_4$	-1199.358	-0.7221
UCl_3	-1058.957	-1.2251
$NdCl_3$	-1228.089	-1.8221

salt (LiCl-$SrCl_2$-CsCl) at a scan rate of 500 mV/s. The cyclic voltammogram (CV) of this base salt from -2.4 V to 1.15 V (vs. the Ag/AgCl reference) shows reduction/oxidation of LiCl at the far left of the range and oxidation of the W electrode at the far right of the range. There are no intermediate potential peaks, due to the fact that Sr^{2+} and Cs^+ reduction potentials are more negative than that of Li^+. Table 6.1 lists the free energies of formation along with calculated standard reduction potentials at 923 K relative to Ag/(1 wt% AgCl).

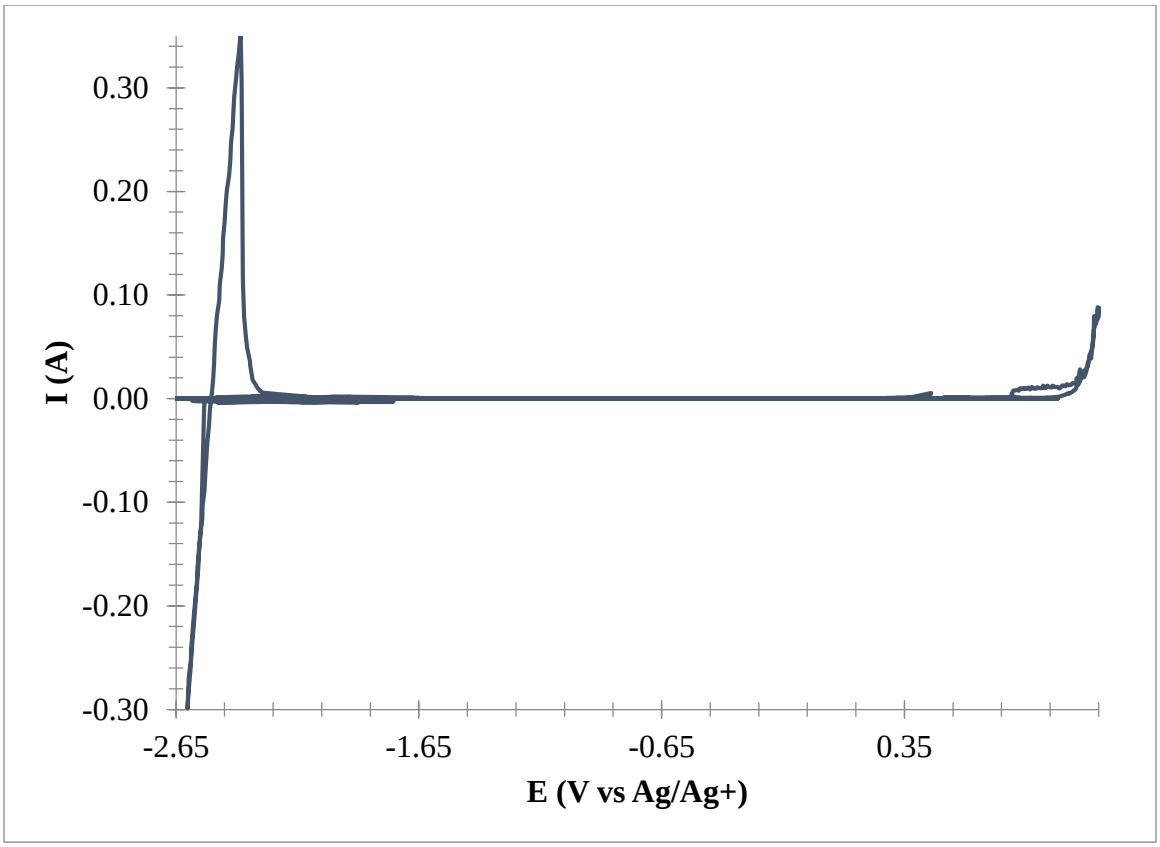

Figure 6.2: Cyclic voltammogram of LiCl-1 wt% $SrCl_2$- 1wt.% CsCl at 923 K.

This indicates that the presence of CsCl and $SrCl_2$, fission products that accumulate in the salt, will not interfere with detection of actinides via electrochemical methods.

After addition UO_2 pellet to the base salt and reaction of $ZrCl_4$ with Zr for one hour, several peaks were recorded during CV analysis. Figure 6.3 shows cyclic voltammogram overlay of scans at various scan rates (150-300 mV/s). A cathodic peak at -1.45 V is observed, which is consistent with the known reduction potential for U^{3+} ions in molten LiCl-KCl salt:[61]

$$B_c: U^{3+} + 3e^- \rightarrow U \qquad (6.1)$$

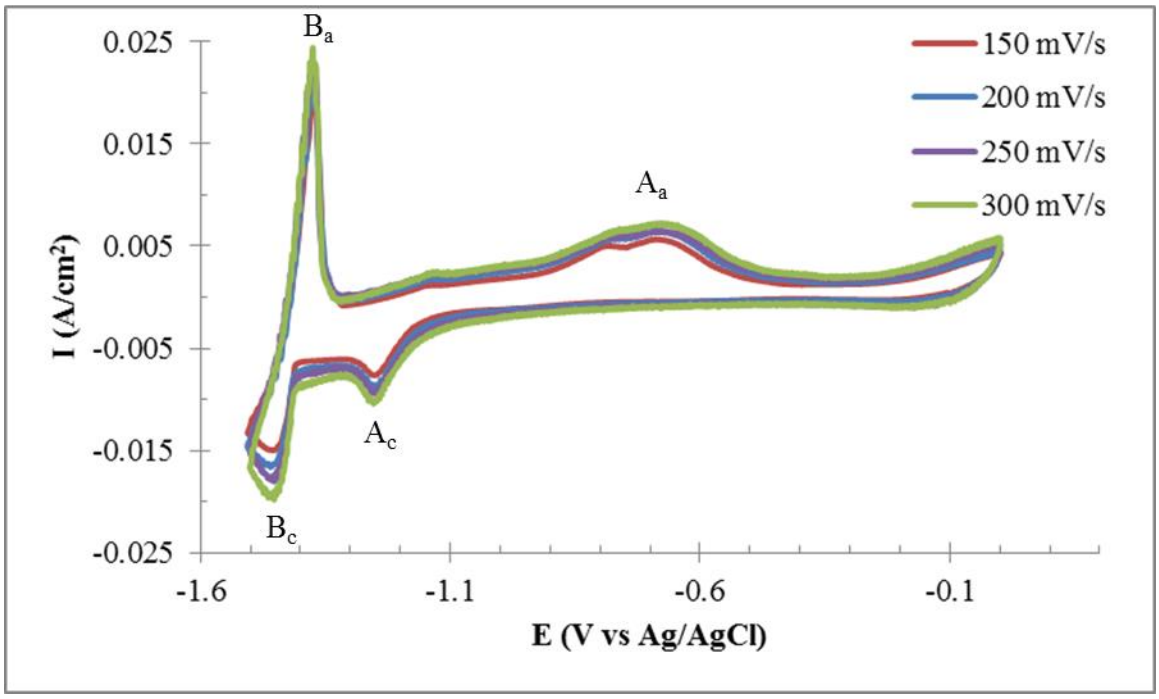

Figure 6.3: Cyclic voltammograms at various scan rates of LiCl-$SrCl_2$-CsCl-UCl_3 after one hour of chlorinating with $ZrCl_4$ and Zr at 923 K.

$$B_c: U^{3+} + 3e^- \rightarrow U \quad (6.1)$$

This is an indication of a small amount of UO_2 being chlorinated to UCl_3. Based on literature, the cathodic peak at -1.25 V is identified as a Zr(IV) reduction to Zr. At -1.5 V the potential is reversed and first oxidation reaction occurs at – 1.37 V. Uranium metal is oxidized to U(III):

$$B_a: U^0 \rightarrow U^{3+} + 3e^- \quad (6.2)$$

At approximately -0.7 V, an anodic peak occurs. This anodic peak represents the oxidation of Zr to Zr(IV):[63,64]

$$A_a: Zr \rightarrow Zr^{4+} + 4e^- \quad (6.3)$$

After another hour of reacting the molten salt with $ZrCl_4$ with Zr, CV was performed. Figure 6.4 shows the CV recorded at several scan rates. All the aforementioned peaks are observed in higher current densities. Figure 6.5 shows an overlap cyclic voltammograms scanned at 200 mV/s of LiCl-$SrCl_2$-CsCl-UCl_3 after one hour and two hours of chlorinating with $ZrCl_4$ and Zr at 923 K. The overlap shows that a significant higher amount of UO_2 was chlorinated after an addition hour of reaction time. Figures 6.4 and 6.6 show plots peak of current density versus square root of scan rate based on CV data. The linearity of the

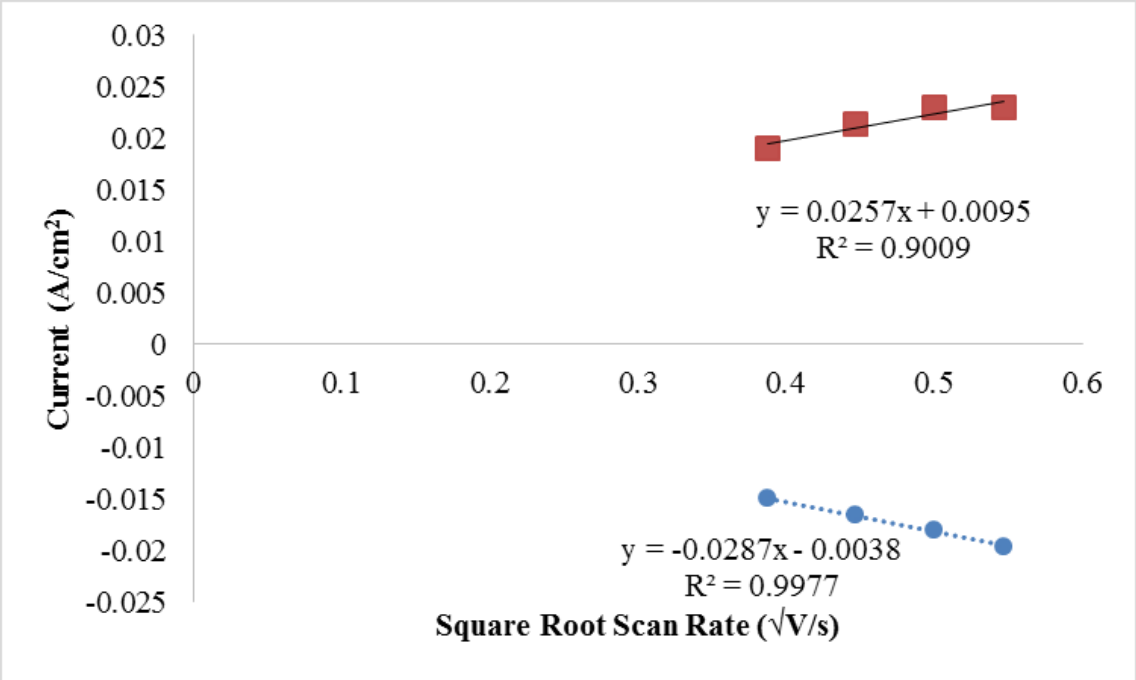

Figure 6.4: Plot of peak current versus square root of scan rate of LiCl-$SrCl_2$-CsCl-UCl_3 salt after one hour of chlorinating at 923 K.

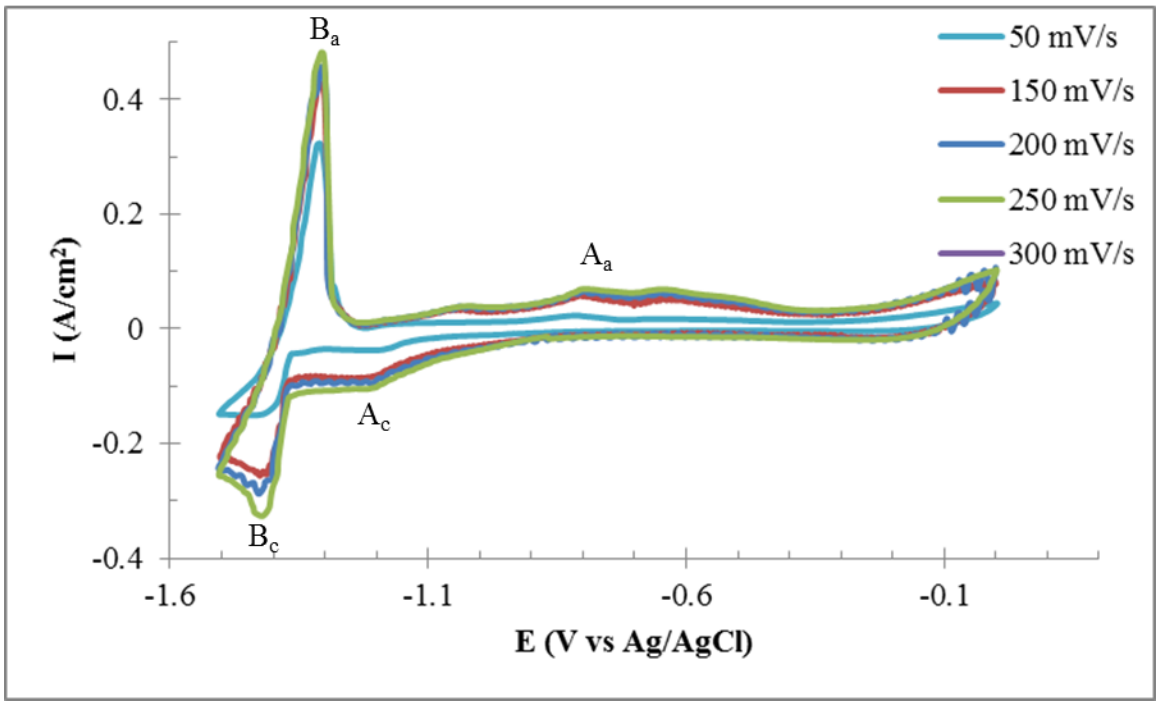

Figure 6.5: Cyclic voltammograms at various scan rates of LiCl-$SrCl_2$-CsCl-UCl_3 after two hours of chlorinating with $ZrCl_4$ and Zr at 923 K.

anodic and cathodic peak current of U(III) indicates the redox reaction is reversible. Additionally, the Berzins-Delahay equation can be applied to the data to obtain the approximate UCl_3 concentration by utilizing the slope of the cathodic peak current density versus square root of scan rate:

$$\frac{I_p}{\sqrt{v}} = 0.6105(nF)^{3/2}(RT)^{-1/2}CS\sqrt{D} \tag{6.4}$$

where I_p is peak current density, v is scan rate, n is number of electrons transferred, F is the Faraday constant, R is the ideal gas constant, T is absolute temperature, C is concentration, S is surface area of the working electrode, and D is diffusivity.

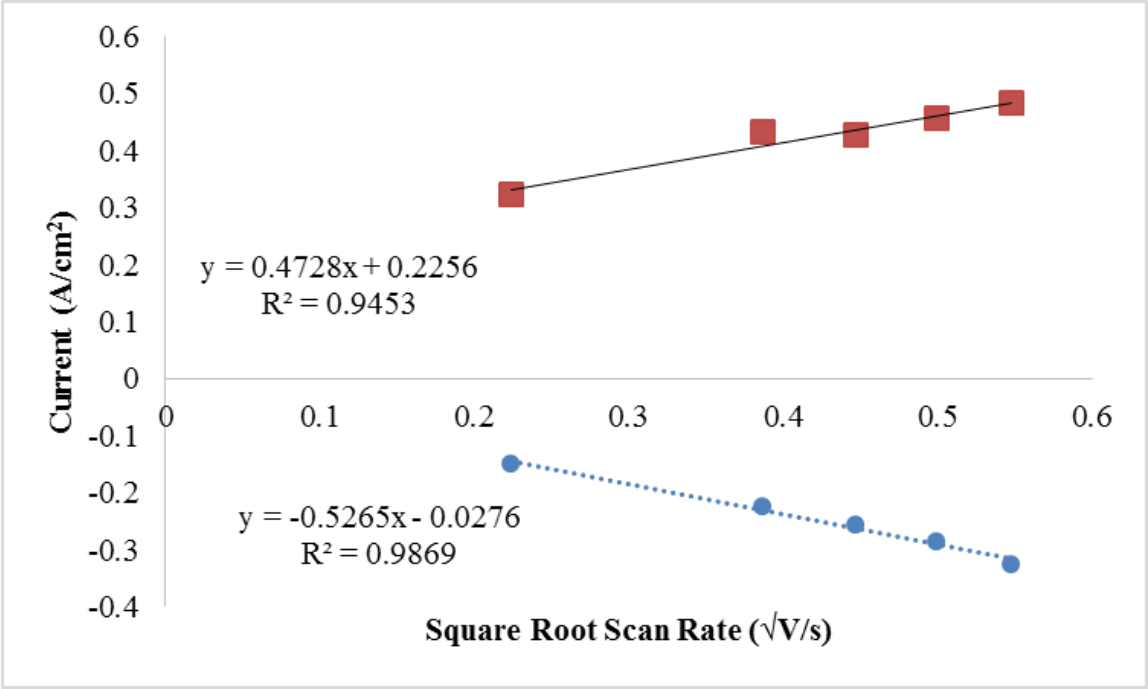

Figure 6.6: Plot of peak current versus square root of scan rate of LiCl-$SrCl_2$-CsCl-UCl_3 salt after two hours of chlorinating at 923 K.

An empirical correlation was used to estimate a diffusion coefficient of 3.295 x 10^{-5} cm^2/sec for U(III) at 923 K.[61] The concentration of UCl_3 after one hour and two hours of chlorination were, thus, calculated to be approximately 6.31 x 10^{-6} and 2.17 x 10^{-4} mol/ml, respectively.

Ultimately, the element of most interest for nonproliferation is plutonium. In spent fuel, there would be approximately 1-10 wt% PuO_2 with a balance of UO_2. The CVs shown in Figures 6.3, 6.5, and 6.7 demonstrate that uranium can readily be detected in the salt after a chlorination process using $ZrCl_4$. Similar experiments cannot be performed at the university with PuO_2, because plutonium is too hazardous to handle. The thermodynamic stability and electrochemical reduction potential of plutonium compounds are similar to rare earths. Thus, chlorination of spent fuel with PuO_2 present was simulated using a mixture of U_3O_8 and Nd_2O_3. A pellet with a composition of 90 wt% U_3O_8 with 10%

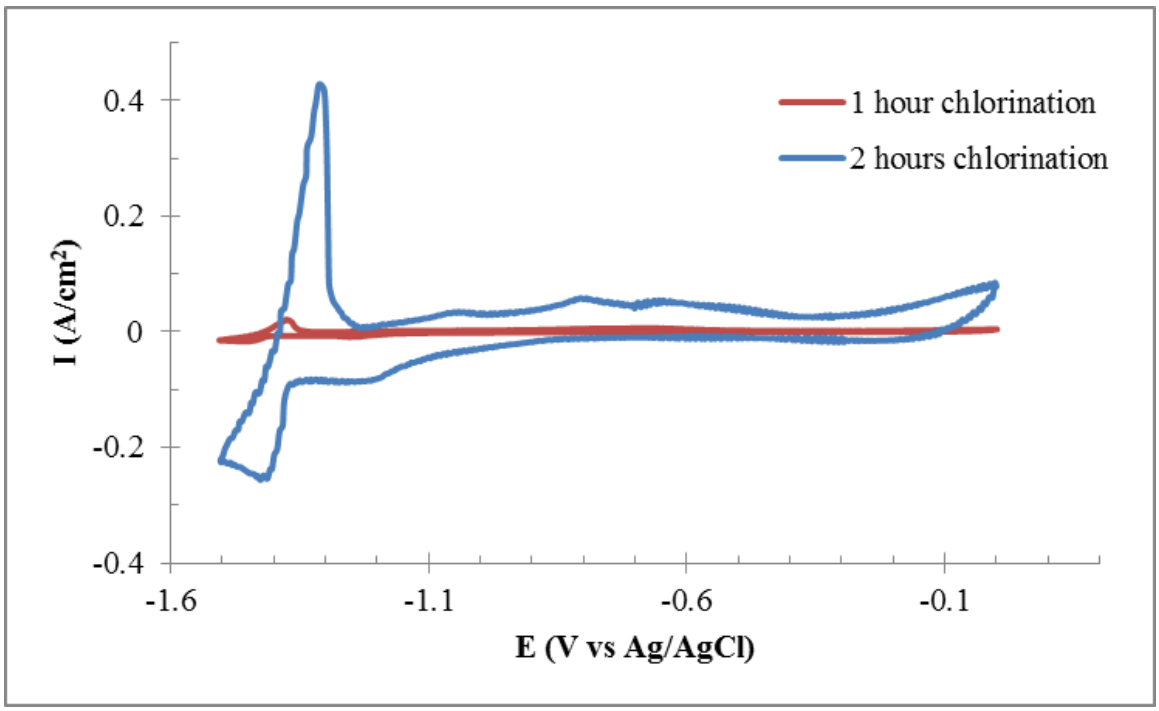

Figure 6.7: Cyclic voltammograms at 200 mV/s scan rate of LiCl-$SrCl_2$-CsCl-UCl_3 after one hour and two hours of chlorinating with $ZrCl_4$ and Zr at 923 K.

Nd_2O_3 was sintered prior to being added to LiCl-$SrCl_2$-CsCl salt. The electrochemical behavior of the salt after one hour of chlorination was recorded. Figure 6.8 shows CV results after chlorination of the salt for one hour with a wide scan window (0.0 to -2.2V) to include Nd peaks. The U(III) cathodic peak is still observed at -1.45 V, and a cathodic peak is visible at -2.15 V which is clearly attributable to Nd(III): [65]

$$C_c: Nd^{3+} + 3e^- \rightarrow Nd \quad (6.5)$$

A Nd(III) anodic peak is subsequently seen at -2.05 V:[65]

$$C_a: Nd \rightarrow Nd^{3+} + 3e^- \quad (6.6)$$

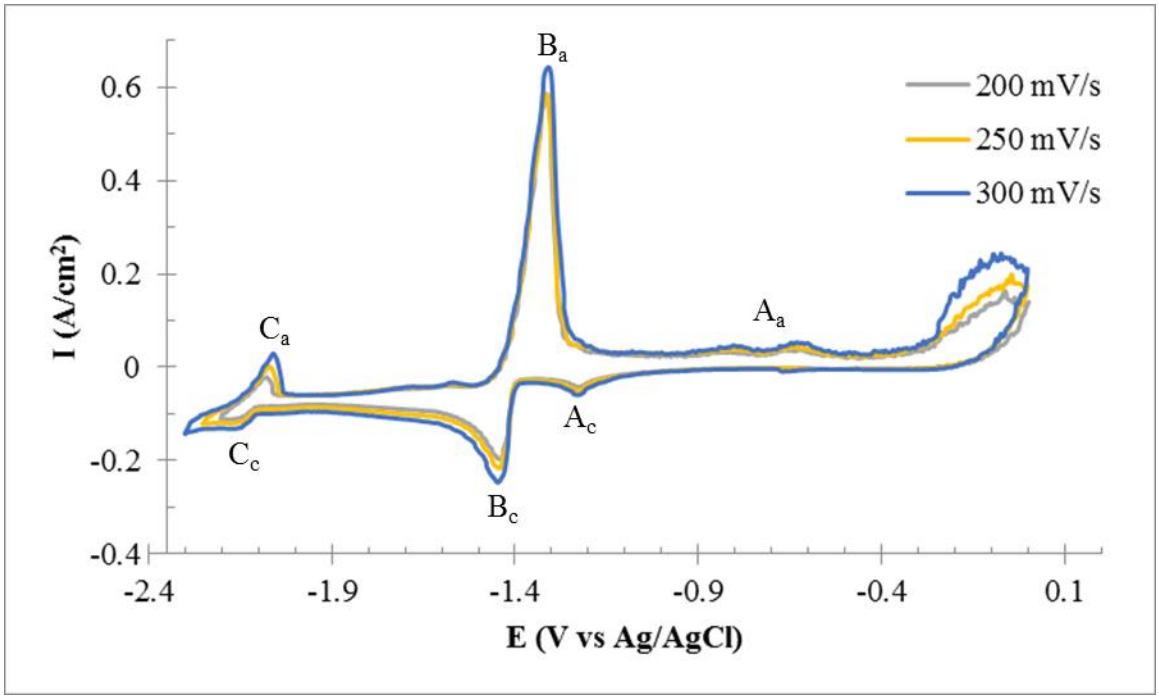

Figure 6.8: Cyclic voltammograms at various scan rates of LiCl-$SrCl_2$-CsCl-UCl_3-$NdCl_3$ after one hour of chlorinating with $ZrCl_4$ and Zr at 923 K.

The only effect observed of Nd_2O_3 to the CV results is noise interference mostly at the positive end of the CV. This noise is likely due to suspended particles in solution being polarized during the potential sweep and attaching to the working and/or counter electrode.

Figure 6.9 shows a plots of U(III) current density versus square root of scan rate based on CV data. The linearity of the anodic and cathodic peak current of U(III) indicates the redox reaction is reversible. Additionally, application of Berzins-Delahay equation to the cathodic peak currents yields an approximate UCl_3 concentration of 1.23 x 10^{-4} mol/ml. Figure 6.10 shows a plots of Nd(III) current density versus square root of scan rate based on CV data in Figure 6.8. The linearity of the anodic and cathodic peak current of Nd(III) indicates the redox reaction is reversible. Additionally, application of Berzins-Delahay equation to the cathodic peak currents using an estimated diffusion coefficient of 1.66 x

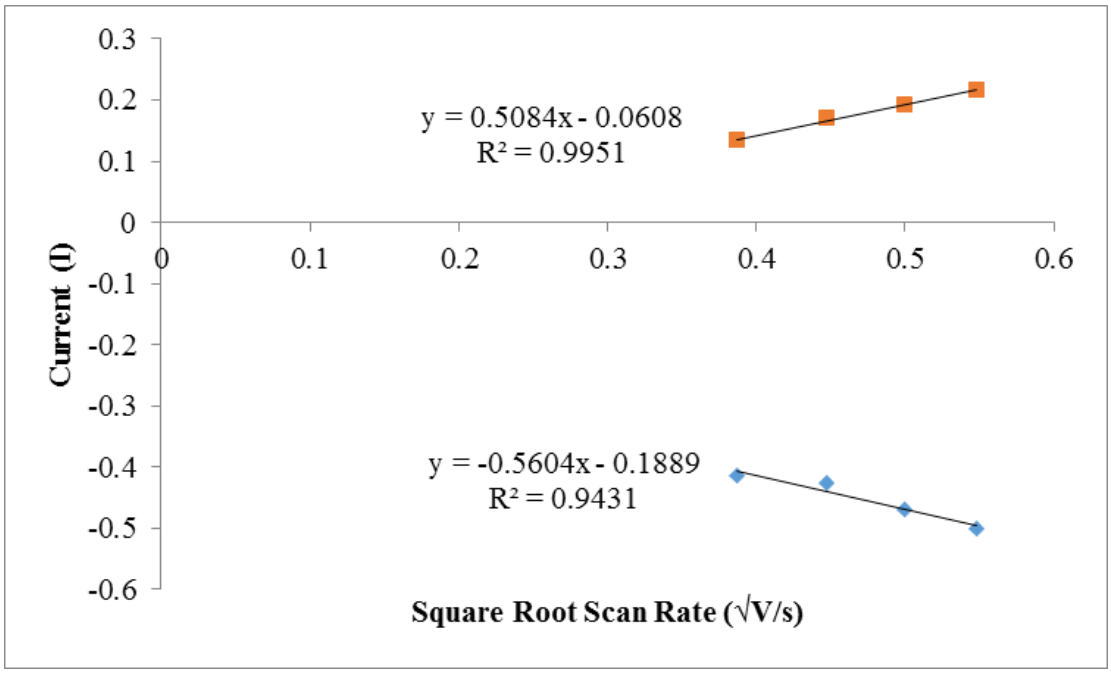

Figure 6.9: Plot of U(III) peak current versus square root of scan rate of LiCl-SrCl2-CsCl-UCl_3-$NdCl_3$ salt after one hour of chlorinating at 923 K.

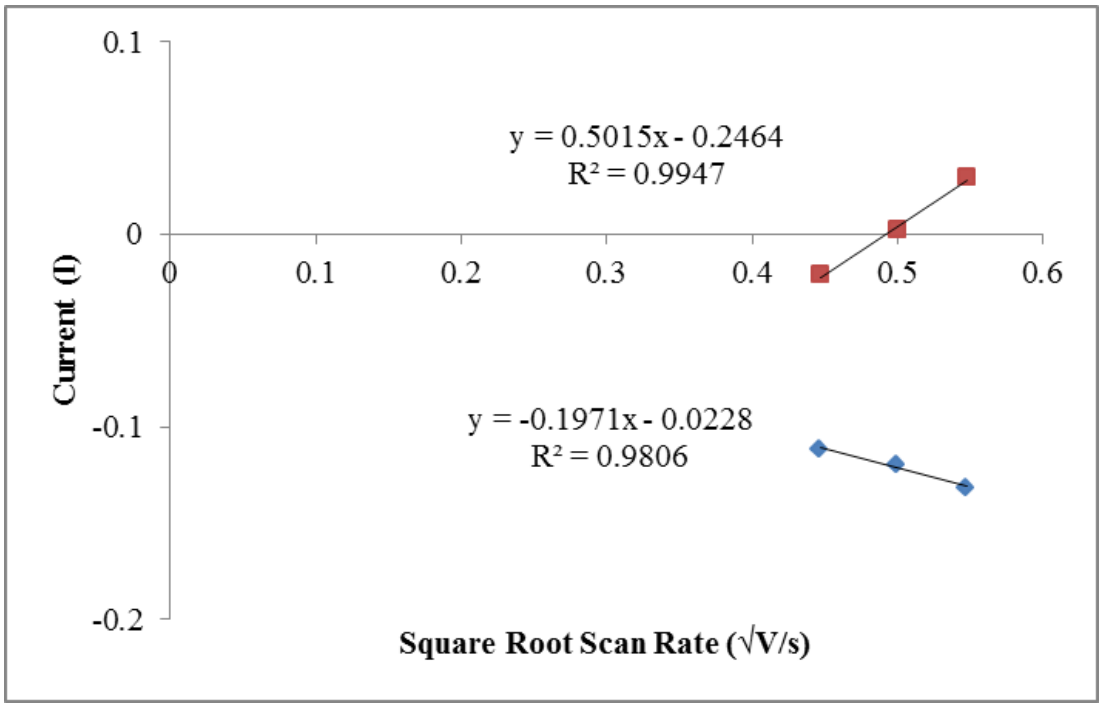

Figure 6.10: Plot of Nd(III) peak current versus square root of scan rate of LiCl-$SrCl_2$-CsCl-UCl_3-$NdCl_3$ salt after one hour of chlorinating at 923 K.

10^{-6} cm/sec yields an approximate $NdCl_3$ concentration of 1.93 x 10^{-4} mol/ml.[61]

Inductively coupled plasma atomic emission spectroscopy (ICP-AES) was used to analysis the concentration levels of UCl_3 and $NdCl_3$. Table 6.2 shows that the chemical analysis follow the pattern calculated by fitting the Berzins-Delahay equation to the cathodic peaks of UCl_3 and $NdCl_3$.

6.3 Thermal Analysis

Differential scanning calorimetry (DSC) analysis was also performed on each of the salt samples. Such a system could readily be utilized by IAEA inspectors to perform thermal analysis of samples of salt taken from a DER system. Phase changes can be determined as a function of temperature using DSC. And the phase behavior of fused salts is typically influenced by the presence and concentration of additives. It was, thus, into the molten salt. Figure 6.11 shows the heat flow graphs for two samples of LiCl plotted speculated that DSC could be used to detect the partitioning of uranium from the fuel basket

Table 6.2: Comparison of ICP-AES analysis and Berzins-Delahay equation fitting results for LiCl-CsCl-$SrCl_2$-UCl_3 after one hour of chlorination, LiCl-CsCl-$SrCl_2$-UCl_3 after two hours of chlorination and LiCl-CsCl-$SrCl_2$-UCl_3-$NdCl_3$ after one hour of chlorination.

	ICP-AES		**Berzins-Delahay Equation**	
Salt	**UCl_3 (mol/cm^3)**	**$NdCl_3$ (mol/cm^3)**	**UCl_3 (mol/cm^3)**	**$NdCl_3$ (mol/cm^3)**
LiCl-CsCl-$SrCl_2$-UCl_3 (I)	1.01E-05	0	2.93E-05	0
LiCl-CsCl-$SrCl_2$-UCl_3 (II)	6.92E-05	0	5.38E-04	0
LiCl-CsCl-$SrCl_2$-UCl_3-$NdCl_3$	3.56E-05	3.56E-05	5.73E-04	3.70E-04

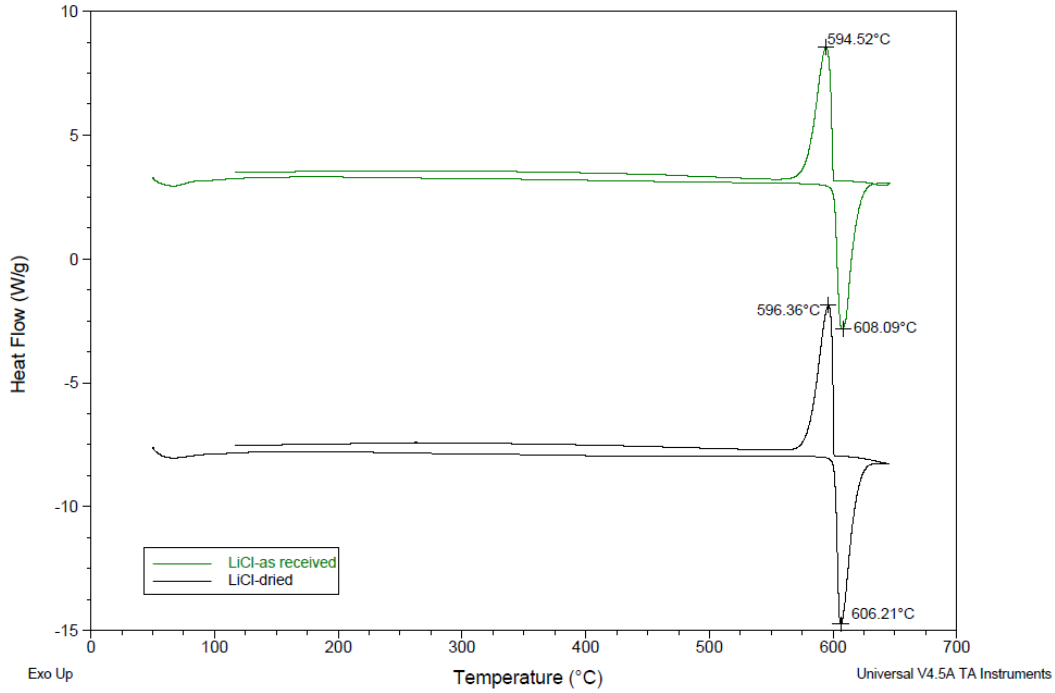

Figure 6.11: DSC result of as-received LiCl and dried LiCl. DSC heated at 10 K/min to 923 K.

versus temperature. In these DSC runs, the temperature was linearly increased at 10 K/min to 923 K and then decreased linearly at 10 K/min back to 323 K. Peaks in the positive direction are representative of exothermic transitions, and negative peaks represent endothermic transitions. In each of these graphs, both peaks coincide with the LiCl liquidus temperature. The comparison of samples in Figure 6.11 is for as-received LiCl and muffle furnace dried LiCl. The peak transition temperatures are not affected the drying process. Pure anhydrous LiCl is known to have a melting point of 878 K (605ºC). The DSC analyses yield consistent peaks at 879 K (606ºC) for dried LiCl and 880 K (608ºC) for as-received LiCl. Figure 6.12 shows TGA data from both dried and as-received LiCl. Data does indicate a mass loss during heat of as-received LiCl. This mass loss is likely residual water.

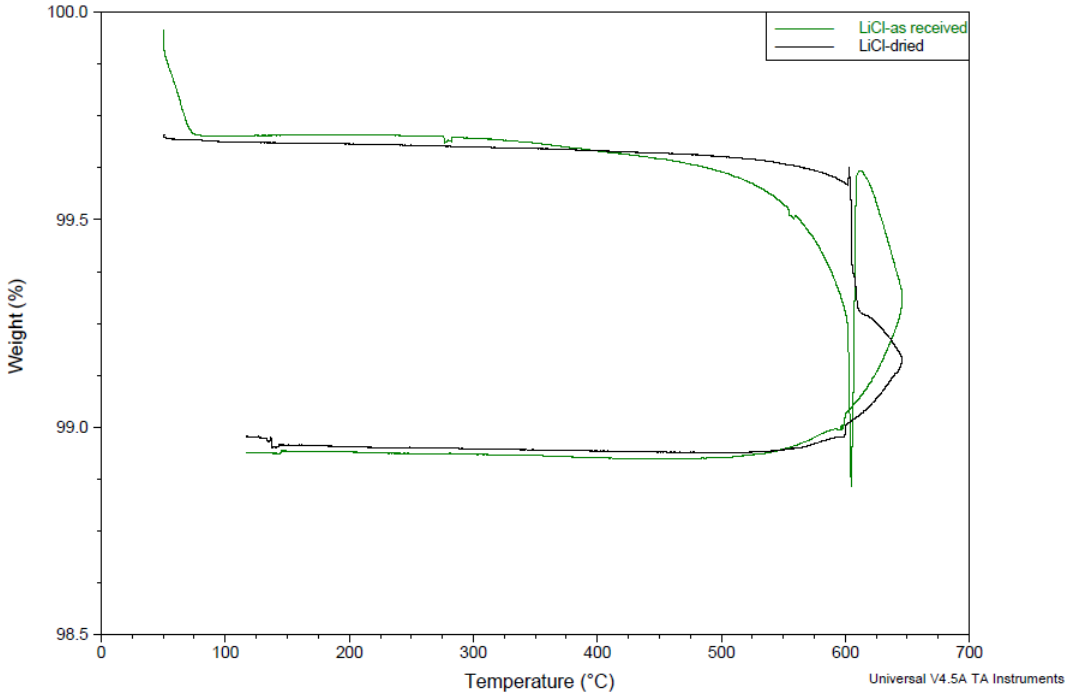

Figure 6.12: TGA data from as-received LiCl and dried LiCl.

Figure 6.13 shows an overlay of the DSC heat flow graphs of dried LiCl, LiCl-1% $SrCl_2$ – 1% CsCl, and LiCl-1% $SrCl_2$ – 1% CsCl-$ZrCl_4$. Most of the peaks exhibit insignificant shifting for these samples. The only exception appears to be the pure LiCl sample, which has an endothermic peak on the heating curve at about 6 K higher than the others. Such small changes in temperature for the observable transitions are difficult to use for the purpose of detecting changes in the salt. Furthermore, there are no secondary peaks evident in these scans. For all practical purposes, DSC cannot differentiate between these three different salts. Figure 6.14 depicts the DSC data for salts containing varying concentrations of UCl_3 and also shows no significant difference in the heat flow. Peaks are not significantly shifted relative to each other. Similarly, Figure 6.15 depicts the DSC data for salt containing UCl3 and NdCl¬3 and also shows no significant shifting of the peak for

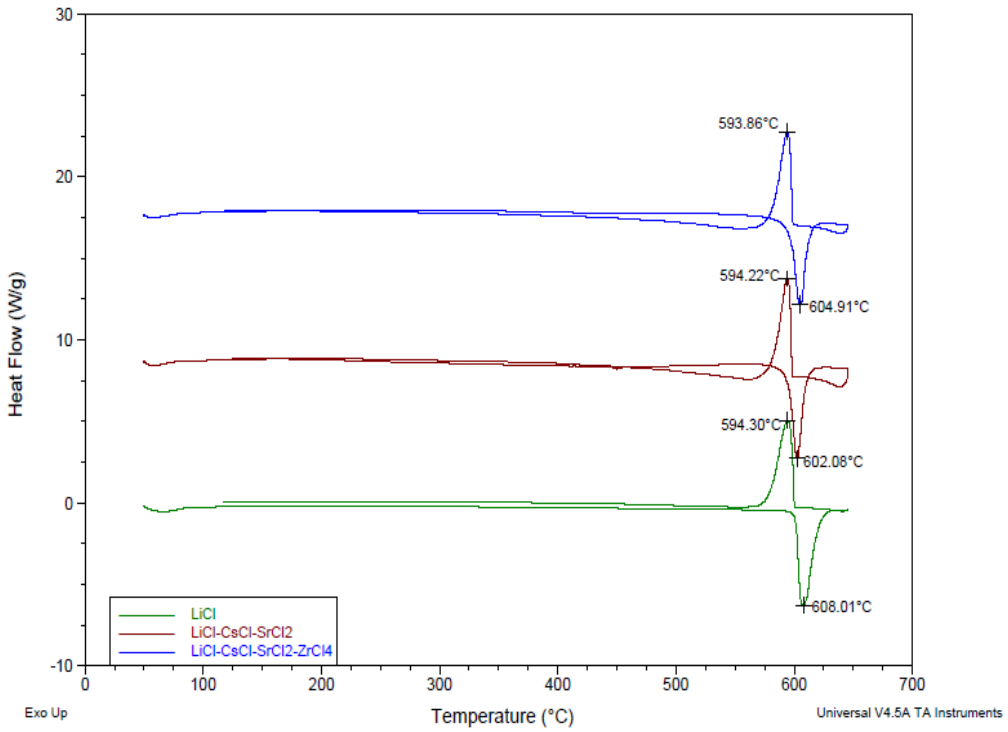

Figure 6.13: DSC result of as-received LiCl, LiCl-1 wt% $SrCl_2$ – 1 wt% CsCl and LiCl-$SrCl_2$-CsCl-$ZrCl_4$ salts. DSC heated at 10 K/min to 923 K.

the various salt compositions.

Based on these DSC results, it is concluded that this type of calorimetry technique would be relatively ineffective in safeguarding of DER salt. The timelessness of the method is already a major drawback since radioactive samples would need to be removed from the hot cell to be analyzed by DSC. Instruments with integrated electronics such as a DSC cannot be operated in a nuclear material hot cell because of the effect of radiation on these instruments. Salt liquidus temperatures are not substantially impacted by the changes in composition that would coincide with attempts to divert plutonium. Thus this type of data would likely not be useful for processing monitor (PM) or signature-based safeguard (SBS) methods.

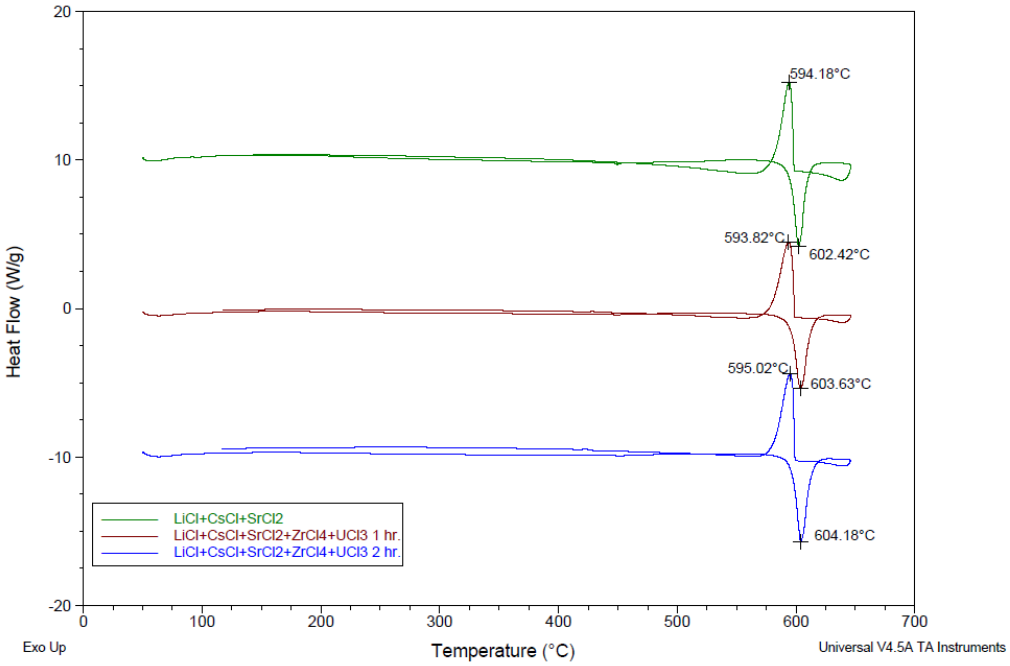

Figure 6.14: DSC results of LiCl-$SrCl_2$-CsCl and LiCl-SrCl2-CsCl-$ZrCl_4$-UCl_3 salt after one hour and two hours of chlorination. DSC heated at 10 K/min to 923 K.

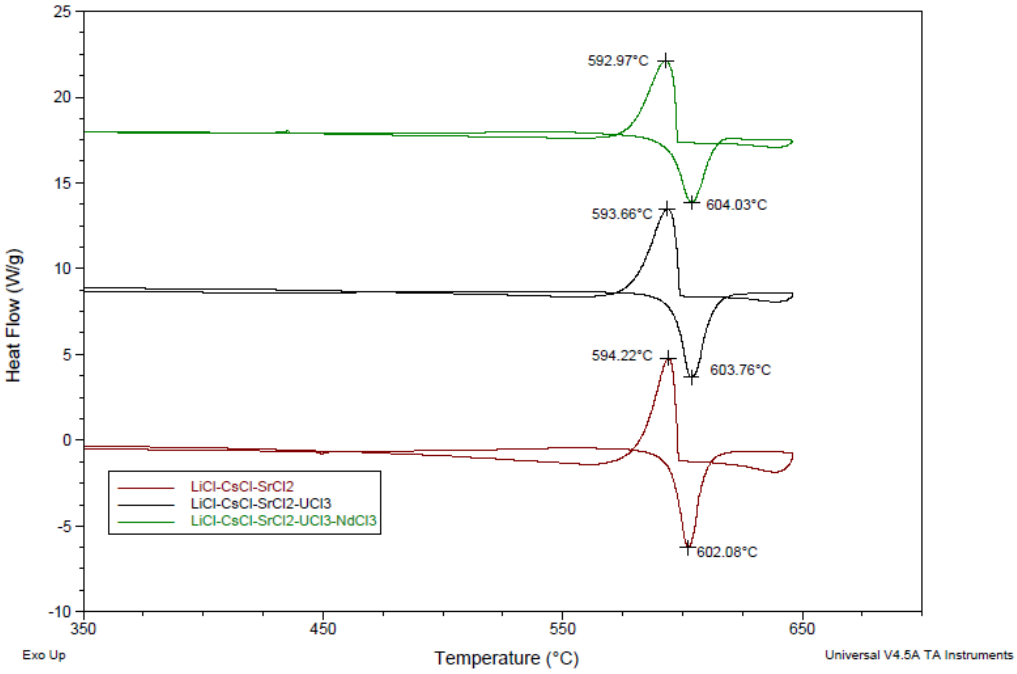

Figure 6.15: DSC results of LiCl-$SrCl_2$-CsCl, LiCl-$SrCl_2$-CsCl-$ZrCl_4$-UCl_3 salt after one hour of chlorination and LiCl-$SrCl_2$-CsCl-$ZrCl_4$-UCl_3-$NdCl_3$ salt after one hour of chlorination. DSC heated at 10 K/min to 923 K.

6.4 UV-Vis Spectroscopy

UV-vis spectroscopy of LiCl was attempted. Obtaining UV-vis spectra of molten salt was very problematic. Quartz cuvettes were required for containment of the salt. Quartz cuvettes are constructed of several thin rectangular pieces of quartz that are fused together. A quartz tube is added to the open end of the quartz cuvette to extend its height; this is known as a graded seal. The fused thin sections of the cuvette tend to fail under high temperature. Quartz cuvettes would often crack and leak molten salt out during heating up to 923 K in the vertical tube furnace. Additionally, the occasional cuvette that did not crack during UV-vis spectroscopy experimentation did crack during cool down. This was likely caused by mechanical stress from the solidification of the LiCl-based salt. Thus, the cuvettes are single use. Additionally, quartz cuvettes are etched by Li_2O; therefore, for true DER safeguard monitoring a different material would be required.

The dimension of the furnace also presented a problem. The furnace had a 25 cm (10 inch) diameter. This not only took up already minimal space in the glovebox but also introduced optical alignment issues. The long focal length resulted in the light beam diverging and creating a large spot size at the outlet. To capture the majority a large collimating lens was required. Through the middle of the furnace were two holes acting as optical windows for the passage of light. These optical windows were machined but not perfectly aligned, thus passing light through the furnace necessitated very fine adjustment in the position of both optical posts.

The modular light source and spectrometer located within the glovebox were unstable. The light source often lost its UV output and the signal processed by the spectrometer fluctuated. This instability is likely due to evaluated temperature (353-383 K)

and static charge within the glovebox.

Overall, all these issues resulted in irregular spectra that were deemed meaningless. Likely some issues can be resolved with the current setup by placing the light source and spectrometer outside the glovebox and channeling the light input and output via fiber optic feedthroughs.

CHAPTER 7

SUMMARY

The extension of nuclear power is being explored by many countries as a sustainable source of energy. A key technical issue facing nuclear power sustainability is management of spent nuclear fuel (SNF). The option of direct disposal of SNF nuclear fuel is not palatable to the public. Thus, countries such as the United States, United Kingdom, France, Germany, Japan, South Korea, India, and Russia are researching reprocessing of spent nuclear fuel. One technology that is being developed for this purpose is pyroprocessing. Pyroprocessing is a high-temperature electrochemical and chemical processing that utilizes molten salt electrolyte. The major benefits of pyroprocessing over traditional hydrometallurgical processing are: no radioactive liquid waste is generated; all radioactive wastes streams are solid at ambient temperatures and readily convertible into stable waste forms; and the inability to generate weapons grade plutonium.

A major component of pyroprocessing spent oxide fuel is direct electrolytic reduction (DER). DER is a necessary head end process for reprocessing of spent oxide fuel that globally makes up the majority of nuclear power reactors. This process involves declad oxide fuel being reduced to a metal in a molten salt consisting of LiCl and 1-3% Li_2O at 923 K. Subsequently, this metallic stream can be reprocessed in an electrorefining step.

Overall, safeguards for pyroprocessing are undeveloped and need to thoroughly design for international acceptance as a viable alternative to PUREX-based reprocessing. In Chapter 2, an extensive literature review discussed various safeguard technologies and their applicability to pyroprocessing. There are three major methodologies of safeguarding nuclear material. Nuclear material accountancy (NMA) is the traditionally mass balance approach has been used in reprocessing and accepted for international safeguard protocols. It is readily applicable in a PUREX-based process; however, it cannot be applied to pyroprocessing due to the nature of eletrorefiner salt holding up actinides. An alternative that is applicable to pyroprocessing is process monitor (PM). PM entails analysis of real-time signals from various reprocessing unit operations. Process control measurements such as flowrates, density measurements, and concentrations can be monitored. Once a data set with normal activity signals is established, a comparison can be made to real-time signals. Analyzing the output measurements of multiple sensors through a statistical algorithm would detect abnormal operations.

A more advance methodology building up PM is signature-based safeguards (SBS). SBS aims to incorporate potential diversion scenarios into physics-based models rather than using statistical inferences. By using physics-based models, there is the potential to minimize false alarms and to more accurately pinpoint anomalous activity. In addition to processing signal being analyzed, data would be collected from electrochemical, gamma, and neutron monitoring.

The focal point of this thesis is to address safeguarding of the oxide reduction process. Oxide reduction has a potential high risk for misuse and diversion of nuclear material if not monitored precisely and regularly. A credible diversion scenario is the

chlorination of uranium and plutonium oxide. An operator could add a reactive chloride species to a DER melt which could hypothetically cause actinide oxides to chlorinate. Table 7.1 highlights the chlorinating agents that were consider and examined for viability using HSC 7.1. $ZrCl_4$ in combination with Zr was chosen for experimental testing of this diversion. A potential benefit to proliferator of using zirconium compound is that zirconium is often present in fuel cladding and thus could be used as an explanation for its presence in DER salt. Furthermore, $ZrCl_4$ high vapor pressure would cause the majority of unreacted $ZrCl_4$ to sublimate out of the salt.

A UV-vis absorption spectroscopy method was explored for examining the content of DER salt. Each chemical species has a unique electronic configuration which is excited by particular energy of light. Consequently, when a known spectrum of light is passed through a sample, the species present and their concentration can be deduced. As Chapter 3 shows, UV-vis spectroscopy had been applied to gauge the concentration of various transition metal, lanthanides, and actinides. A UV-vis spectroscopy setup was devised for experimentation of this technique. However, no legitimate spectra were obtained throughout the experimentation. The major issues encountered in UV-vis experimentation were the fragility of quartz cuvettes and the inability to obtain a stable signal to the spectrometer.

Another safeguard monitoring technique explored for detection of diversion in DER salt was electrochemical analysis. A review of past research and theoretical bases was given in Chapter 4. Cyclic voltammetry (CV) was chosen as the main technique for analysis of DER salt. Cyclic voltammetry (CV) is a common electrochemical where a potential is ramped at a constant scan rate between two vertex potentials. This potential sweep method

Table 7.1: List of chlorinating agents considered for reaction with actinide oxides. Gibb's free energy of reaction and vapor pressures of the various chlorinating agents are given at 923 K.

Chlorinating Agent	P_{sat} (atm)	Reaction	ΔG (kJ)
VCl_3	1.45E+00	$3PuO_2 + 3VCl_3 + V = 3PuCl_3 + 2V_2O_3$	-4.61E+02
		$3UO_2 + 3VCl_3 + V = 3UCl_3 + 2V_2O_3$	-6.56E+01
		$3U_3O_8 + 9VCl_3 + 7V = 9UCl_3 + 8V_2O_3$	-5.36E+02
$AlCl_3$	1.38E+01	$3PuO_2 + 3AlCl_3 + Al = 3PuCl_3 + 2Al_2O_3$	-8.43E+02
		$3UO_2 + 3AlCl_3 + Al = 3UCl_3 + 2Al_2O_3$	-4.47E+02
		$3U_3O_8 + 9AlCl_3 + 7Al = 9UCl_3 + 8Al_2O_3$	-1.19E+03
WCl_6	4.82E+01	$2PuO_2 + WCl_6 + W = 2PuCl_3 + 2WO_2$	-3.74E+02
		$2UO_2 + WCl_6 + W = 2UCl_3 + 2WO_2$	-1.10E+02
		$2U_3O_8 + 3WCl_6 + 5W = 6UCl_3 + 8WO_2$	-4.02E+02
$TiCl_4$	4.01E+03	$4PuO_2 + 3TiCl_4 + 5Ti = 4PuCl_3 + 8TiO$	-4.54E+02
		$4UO_2 + 3TiCl_4 + 5Ti = 4UCl_3 + 8TiO$	-2.78E+02
		$4U_3O_8 + 9TiCl_4 + 23Ti = 12UCl_3 + 32TiO$	-1.35E+03
$ThCl_4$	3.75E-03	$4PuO_2 + 3ThCl_4 + Th = 4PuCl_3 + 4ThO_2$	-9.64E+02
		$4UO_2 + 3ThCl_4 + Th = 4UCl_3 + 4ThO_2$	-4.36E+02
		$4U_3O_8 + 9ThCl_4 + 7Th = 12UCl_3 + 18ThO_2$	-1.20E+03
$ZrCl_4$	9.29E+02	$4PuO_2 + 3ZrCl_4 + Zr = 4PuCl_3 + 4ZrO_2$	-1.07E+03
		$4UO_2 + 3ZrCl_4 + Zr = 4UCl_3 + 4ZrO_2$	-5.37E+02
		$4U_3O_8 + 9ZrCl_4 + 7Zr = 12UCl_3 + 16ZrO_2$	-1.14E+03

can be used to diagnose electrochemical reaction mechanisms, identify electroactive species present, and indicate relative concentrations of ionic species by resulting current response. CV data showed that $ZrCl_4$ with Zr could chlorinate UO_2 and UO_2/Nd_2O_3 as UCl_3 and $NdCl_3$. Analysis of the CV with the Berzins-Delahay equation showed that after two hours of chlorination, 2.17×10^{-4} mol/ml of UCl_3 was present in the LiCl-based salt. Additionally, when a mixed pellet of UO_2 and Nd_2O_3 was chlorinated for one hour, 1.23×10^{-4} mol/ml of UCl_3 and 1.93×10^{-4} mol/ml of $NdCl_3$ were present in the salt.

In conclusion, the hypothetical diversion scenario for the direct electrolytic reduction process has been experimentally verified (using Nd_2O_3 as a surrogate for PuO_2). Furthermore electrochemical analysis (voltammetry) has proven to be the best method to detect the diversion attempt.

REFERENCES

(1) Nuclear | Department of Energy http://energy.gov/science-innovation/energy-sources/nuclear (accessed Jun 26, 2014).

(2) Andrews, A. *Nuclear Fuel Reprocessing: US Policy Development*; CRS Report for Congress RS22542; DTIC Document, 2006.

(3) Gaffigan, M. E. *Effects of a Termination of the Yucca Mountain Repository Program and Lessons Learned*; GAO-11-229, US Government Accountability Office, 2011.

(4) Bruno, J.; Ewing, R. C. *Elements* **2006**, *2*, 343–349.

(5) Doyle, J. E. *Nuclear safeguards, security and nonproliferation : achieving security with technology and policy*; Butterworth-Heinemann: Amsterdam; Boston, 2008.

(6) Mathur, J. N.; Murali, M. S.; Nash, K. L. *Solvent Extr. Ion Exch.* **2001**, *19*, 357–390.

(7) Poineau, F.; Du Mazaubrun, J.; Ford, D.; Fortner, J.; Kropf, J.; Silva, G. W. C.; Smith, N.; Long, K.; Jarvinen, G.; Czerwinski, K. R. *Radiochim. Acta* **2008**, *96*.

(8) Serrano-Purroy, D.; Baron, P.; Christiansen, B.; Malmbeck, R.; Sorel, C.; Glatz, J.-P. *Radiochim. Acta* **2005**, *93*.

(9) Magnusson, D.; Christiansen, B.; Foreman, M. R. S.; Geist, A.; Glatz, J. -P.; Malmbeck, R.; Modolo, G.; Serrano-Purroy, D.; Sorel, C. *Solvent Extr. Ion Exch.* **2009**, *27*, 97–106.

(10) Law, J. D.; Herbst, R. S.; Todd, T. A.; Romanovskiy, V. N.; Babain, V. A.; Esimantovskiy, V. M.; Smirnov, I. V.; Zaitsev, B. N. *Solvent Extr. Ion Exch.* **2001**, *19*, 23–36.

(11) Herrmann, S. D.; Li, S. X. *Nucl. Technol.* **2010**, *171*, 247.

(12) National Research Council, Committee on Electrometallurgical Techniques for DOE Spent Fuel Treatment. *Electrometallurgical Techniques for DOE Spent Fuel Treatment;* Washington, D.C., 2000, 1-116.

(13) Herrmann, S. D.; Li, S. X.; Westphal, B. R. *Sep. Sci. Technol.* **2012**, *47*, 2044–2059.

(14) Inoue, T.; Koch, L. *Nucl. Eng. Technol.* **2008**, *40*, 183.

(15) Herrmann, S. D.; Li, S. X.; Simpson, M. F.; Phongikaroon, S. *Sep. Sci. Technol.* **2006**, *41*, 1965–1983.

(16) Goode, J. H. *Voloxidation: removal of volatile fission products from spent LMFBR fuels.*; ORNL-TM-3723, Oak Ridge National Lab, TN, 1973; 1-135.

(17) Karen, E.J.; Gourishankar, K.V. *Electrometallurgical Treatment of Oxide Spent Fuel–Engineering Scale Development.* In Third Topical Meeting on DOE Spent Nuclear Fuel and Fissile Materials Management, Charleston, SC, 1998.

(18) Simpson, M. F.; Rappleye, D.; Blandford, E. D.; Garcia, H. Proceedings of the 2014 INMM Annual Meeting, Atlanta, GA, July 20-24, 2014.

(19) Pellechi, M.; Chimedbazaryn, J.; Hori, A.; Lebrun, S.; Li, S.; Petoe, A.; Hussin, S. S.; Zarucki, R. In *Proceedings of the Institute of Nuclear Materials Management 52nd*; Institute of Nuclear Materials Management: Palm Desert, California, U.S.A, 2011; pp. 2547–2555.

(20) Cipiti, B. B.; Duran, F. A.; Key, B.; Liu, Y.; Lozano, I.; Ward, R. *Modeling and design of integrated safeguards and security for an electrochemical reprocessing facility*; Sandia National Laboratories, 2012.

(21) *Global Nuclear Energy Partnership Technology Development Plan*; GNEP-TECH-TR-PP-2007-00020.

(22) Lafreniere, P.; Rappleye, D.; Simpson, M. F.; Blandford, E. D. *Nucl. Technol. Accepted*.

(23) Eccleston, G. *Passive/Active Neutron Coincidence Counter*; LALP 93-31; Los Alamos National Laboratory: Los Alamos, NM, 1993.

(24) Bean, R. *Project report on development of a safeguards approach for pyroprocessing;* INL/EXT-10-2005; Idaho National Laboratory: Idaho Falls, ID 2010; 1-30.

(25) Hansen, J. S. *APPLICATION GUIDE TO TOMOGRAPHIC GAMMA SCANNING OF URANIUM AND PLUTONIUM*; LA-UR-04-7014; Los Alamos National Laboratory: Los Alamos, NM; 1–55.

(26) *Portable X-Ray, K-Edge Heavy Metal Detector*; Innovative Technology Summary Report DOE/EM-0519; DOE, Office of Environment Management: Office of Science and Technology, 2000; 1–41.

(27) Kim, B. Y.; Lee, D. H.; Lee, J.-Y.; Yun, J.-I. *Electrochem. Commun.* **2010**, *12*, 1005–1008.

(28) Hanson, C.; Phongikaroon, S.; Scott, J. R. *Spectrochim. Acta Part B At. Spectrosc.* **2014**, *97*, 79–85.

(29) Park, Y. J.; Bae, S. E.; Cho, Y. H.; Kim, J. Y.; Song, K. *Microchem. J.* **2011**, *99*, 170–173.

(30) Fujii, T.; Uda, T.; Fukasawa, K.; Uehara, A.; Sato, N.; Nagai, T.; Kinoshita, K.; Koyama, T.; Yamana, H. *J. Radioanal. Nucl. Chem.* **2013**, *296*, 255–259.

(31) Fukushima, K.; Yamoto, H.; Iwadate, Y. *J. Alloys Compd.* **1999**, *290*, 114–118.

(32) Wallace, P. D. R.; Therios, I.; Ehinger, M. H.; Bean, R.; Kovacic, D. N.; Tolk, A. D. K.; Boyer, B. **2007**.

(33) Bard, A. J.; Faulkner, L. R. *Electrochemical Methods: Fundamentals and Applications*; Wiley, 2000.

(34) Sridharan, K.; Martin, S.; Mohammadian, M.; Sager, J.; Allen, T.; Simpson, M. *Trans. Am. Nucl. Soc.* **2012**, *106*, 1240–1241.

(35) Alonso, J. I. G.; Thoby-Schultzendorff, D.; Giovanonne, B.; Glatz, J.-P.; Pagliosa, G.; Koch, L. *J. Anal. At. Spectrom.* **1994**, *9*, 1209.

(36) Sakamura, Y.; Inoue, T.; Iwai, T.; Moriyama, H. *J. Nucl. Mater.* **2005**, *340*, 39–51.

(37) Fujii, T.; Moriyama, H.; Yamana, H. *J. Alloys Compd.* **2003**, *351*, L6–L9.

(38) Young, J. P.; White, J. C. *Anal. Chem.* **1960**, *32*, 799–802.

(39) Fukasawa, K.; Uehara, A.; Nagai, T.; Fujii, T.; Yamana, H. *J. Nucl. Mater.* **2011**, *414*, 265–269.

(40) Cho, Y.-H.; Bae, S.-E.; Park, Y.-J.; Oh, S.-Y.; Kim, J.-Y.; Song, K. *Microchem. J.* **2012**, *102*, 18–22.

(41) Cho, Y. H.; Kim, T.-J.; Bae, S. E.; Park, Y. J.; Ahn, H. J.; Song, K. *Microchem. J.* **2010**, *96*, 344–347.

(42) Smith, G. P. *Review of electronic absorption spectra of molten salts*; ORNL-3411; U.S. Atomic Energy Commission: Oak Ridge National Laboratory, 1963; 1-66.

(43) Gruen, D. M.; McBeth, R. L. *J. Phys. Chem.* **1962**, *66*, 57–65.

(44) Li, J.; Dasgupta, P. K. *Rev. Sci. Instrum.* **2000**, *71*, 2283.

(45) Gabriel, J. .; Vincent, D.; Bouteillon, J.; Poignet, J. .; Volkovich, V. .; Griffiths, T. . *Electrochimica Acta* **1999**, *44*, 4619–4629.

(46) Suzuki, S.; Tanaka, K. *T. Jpn. I. Met.* **1970**, 11, 324-327.

(47) Oh, S. Y.; Kim, J.-Y.; Bae, S. E.; Cho, Y. H.; Yeon, J.-W.; Song, K. *J. Lumin.* **2013**, *134*, 706–709.

(48) Fujii, T.; Uehara, A.; Nagai, T.; Yamana, H. *Z. Naturforschung -J. Phys. Sci.* **2007**, *62*, 733–738.

(49) Banks, C. V.; Heusinkveld, M. R.; O'Laughlin, J. W. *Anal. Chem.* **1961**, *33*, 1235–1240.

(50) Fukasawa, K.; Uehara, A.; Nagai, T.; Fujii, T.; Yamana, H. *J. Alloys Compd.* **2011**, *509*, 5112–5118.

(51) Fujii, T.; Nagai, T.; Uehara, A.; Yamana, H. *J. Alloys Compd.* **2007**, *441*, L10–L13.

(52) Cho, Y.-H.; Kim, T.-J.; Park, Y.-J.; Im, H.-J.; Song, K. *J. Lumin.* **2010**, *130*, 280–282.

(53) Schroll, C. A.; Chatterjee, S.; Levitskaia, T. G.; Heineman, W. R.; Bryan, S. A. *Anal. Chem.* **2013**, *85*, 9924–9931.

(54) Polovov, I. B.; Sharrad, C. A. A.; May, I.; Vasin, B. D. D.; Volkovich, V. A.; Griffiths, T. R. R. ECS, 2007; Vol. 3, pp. 503–511.

(55) Polovov, I. B.; Volkovich, V. A.; Charnock, J. M.; Kralj, B.; Lewin, R. G.; Kinoshita, H.; May, I.; Sharrad, C. A. *Inorg. Chem.* **2008**, *47*, 7474–7482.

(56) Fujii, T.; Uehara, A.; Nagai, T.; Kim, T.-J.; Sato, N.; Sakamura, Y.; Yamana, H. *Electrochemistry* **2009**, *77*, 667–669.

(57) Gruen, D. M.; Fried, S.; Graf, P.; McBeth, R. L. In *Proceedings of the second United Nations International Conference on the Peaceful Uses of Atomic Energy*; United Nations: Geneva, 1958; pp. 112–119.

(58) Swanson, J. L. *J. Phys. Chem.* **1964**, *68*, 438–439.

(59) Driggs, F. H.; Lilliendahl, W. C. *Ind. Eng. Chem.* **1930**, *22*, 516–519.

(60) Bard, A. J.; Faulkner, L. R. *Hoboken Wiley Sons* **2001**.

(61) Zhang, J. *J. Nucl. Mater.* **2014**, *447*, 271–284.

(62) Kuznetsov, S. A.; Hayashi, H.; Minato, K.; Gaune-Escard, M. *J. Electrochem. Soc.* **2005**, *152*, C203.

(63) Hoover, R. O. Uranium and zirconium electrochemical studies in LiCl-KCl eutectic for fundamental applications in used nuclear fuel reprocessing. Ph.D., University of Idaho: Ann Arbor, 2014.

(64) Sakamura, Y. *J. Electrochem. Soc.* **2004**, *151*, C187.

(65) Masset, P.; Konings, R. J. M.; Malmbeck, R.; Serp, J.; Glatz, J.-P. *J. Nucl. Mater.* **2005**, *344*, 173–179.